Inorganic Chemistry

Article

pubs.acs.org/IC

Flavonolate Complexes of M^{II} (M = Mn, Fe, Co, Ni, Cu, and Zn). Structural and Functional Models for the ES (Enzyme–Substrate) Complex of Quercetin 2,3-Dioxygenase

Ying-Ji Sun,*[,†] Qian-Qian Huang,[†] Tetsuro Tano,[‡] and Shinobu Itoh[‡]

[†]School of Chemistry, Dalian University of Technology, 2 Linggong Road, Dalian 116024, China

[‡]Department of Material and Life Science, Division of Advanced Science and Biotechnology, Graduate School of Engineering, Osaka University, 2-1 Yamada-oka, Suita, Osaka 565-0871, Japan

Supporting Information

ABSTRACT: A series of flavonolate complexes $[M^{II}L(fla)]$ (M = Mn (**1**), Fe (**2**), Co (**3**), Ni (**4**), Cu (**5**), and Zn (**6**), **LH**: 2-{[bis(pyridin-2-ylmethyl)amino]methyl}benzoic acid, fla: flavonolate) have been synthesized as structural and functional models for the ES (enzyme–substrate) complexes of the active site of various M^{II}-containing quercetin 2,3-dioxygenase (2,3-QD) and their structures, spectroscopic features, and redox properties, as well as the reactivity toward molecular oxygen, have been investigated. The metal centers of $[Fe^{II}L(fla)]\cdot H_2O$ (**2**), $[Co^{II}L(fla)]\cdot CH_3OH$ (**3**), and $[Ni^{II}L(fla)]$ (**4**) exhibit a distorted octahedral geometry with two oxygen atoms of fla, one oxygen atom of the benzoate group of ligand L, and three nitrogen atoms of ligand L, in which oxygen atom of the carbonyl group of fla and one of the pyridine nitrogen atoms occupy the axial positions. The complexes $[M^{II}L(fla)]$ exhibit relatively high reactivity in the oxidative ring-opening of the bound flavonolate at lower temperature, presumably due to the existing carboxylate group in the supporting ligand. Thus, our complexes act as good functional ES models of various metal(II)-containing 2,3-QD. In addition, complexes $[Fe^{II}L(fla)]\cdot H_2O$ (**2**), $[Co^{II}L(fla)]\cdot CH_3OH$ (**3**), and $[Ni^{II}L(fla)]$ (**4**) are the first structurally characterized Fe^{II}-, Co^{II}-, and Ni^{II}-flavonolate complexes, as an active site ES model of Fe^{II}-, Co^{II}-, and Ni^{II}-containing 2,3-QD, respectively. The model complexes exhibit notably different reactivity in the order of Fe (**2**) > Cu (**5**) > Co (**3**) > Ni (**4**) > Zn (**6**) > Mn (**1**). The differences in the reactivity among them may be attributed to the redox potential of the coordinated flavonolate of the complexes, which are remarkably influenced by the Lewis acidity of the metal ion and its coordination environment. Our study is the first example of the metal ion effects on the enzyme-like dioxygenation reactivity, providing important insights into the metal ion effects on the enzymatic reactivity of various metal(II)-containing 2,3-QD.

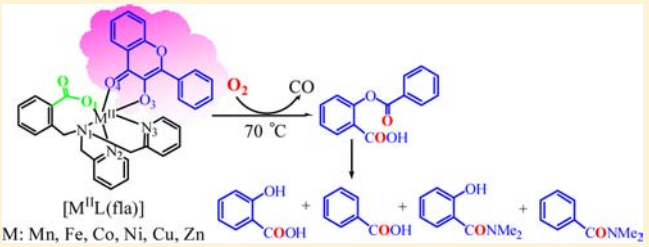

INTRODUCTION

Quercetin 2,3-dioxygenase (2,3-QD) activates molecular oxygen to catalyze the oxygenative ring-opening reaction of the *O*-heterocycle of quercetin (3′,4′,5,7-tetrahydroxyflavonol, QUE) to the corresponding depside (phenolic carboxylic acid esters) and carbon monoxide (Scheme 1).[1]

The mononuclear copper(II) active site of resting 2,3-QD from *Aspergillus japonicus* (homo bicupin glycoprotein) exhibits two distinct geometries: a distorted trigonal-bipyramidal geometry consisting of three histidine imidazoles (His66, His68, and His112), one water molecule and a carboxylate group of Glu73 (*minor* conformation 30%), and a distorted tetrahedral geometry without the direct coordinative interaction between copper(II) ion and the carboxylate group of Glu73 (*major* conformation 70%). In its principal conformation, Glu73 acts as a hydrogen bond acceptor for the metal-bound water molecule.[2] The substrate quercetin is bound to the copper(II) ion through the deprotonated 3-hydroxy group of flavonolate, with displacement of the water molecule, forming an ES (enzyme–substrate) complex with a distorted square pyramidal geometry under anaerobic conditions.[3] The carboxylate group of Glu73 probably acts as an active site base for the deprotonation of the substrate, stabilizes the bound substrate via a hydrogen bonding interaction, modulates the redox potential of the metal ion in the ES adduct, thus lowering the energy barriers.[2,4] The site directed mutagenesis study has indicated that the enzyme is inactive without Glu73.[2]

The active site of Fe^{II}-containing 2,3-QD from *Bacillus subtilis* (hetero bicupin glycoprotein) has been shown to exhibit

Scheme 1

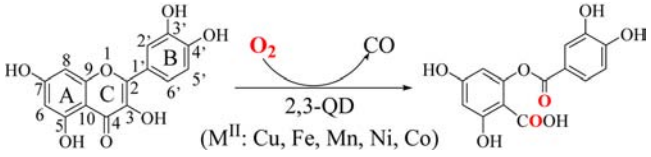

Received: April 19, 2013
Published: September 17, 2013

   dx.doi.org/10.1021/ic400972k | *Inorg. Chem.* 2013, 52, 10936–10948

similar structures. The one has a distorted trigonal-bipyramidal geometry consisting of three histidine imidazoles (His62, His64, and His103), a water molecule and one Glu69 at a 2.10 Å distance in the *N*-terminal cupin motif, and the other has a square pyramidal geometry consisting of three histidine imidazoles (His234, His236, His275), a water molecule, and a weakly coordinating Glu241 at a 2.44 Å distance in the *C*-terminal cupin motif.[5a] Previous metal-replacement experiments have shown that the Mn^{II}- and Co^{II}-containing enzymes were 35- and 24-fold more active than the Fe^{II}-containing native enzyme, respectively. Thus, Mn^{II} is a preferable metal cofactor for 2,3-QD from *B. subtilis*.[6a] The EPR studies indicate that the Mn(II)-containing 2,3-QD from *Bacillus subtilis* has a high-spin ($S = {}^5/_2$) mononuclear Mn(II) center in a octahedral geometry in the resting state.[6a]

On the other hand, recent study of 2,3-QD from *Streptomyces* sp. FLA (monocupin) indicated that the highest and next highest level of reactivity was observed when the enzyme was overexpressed in *E. coli* in the LB medium containing Ni^{II} and Co^{II} salts, but less reactivity was observed with Mn^{II}, Fe^{II}, Cu^{II}, or Zn^{II} salts.[6b] The EPR studies indicate that the Co(II)-containing 2,3-QD from *Streptomyces* sp. FLA has a high-spin ($S = {}^3/_2$) mononuclear Co(II) center in a trigonal bipyramidal or tetrahedral geometry in the resting state.[6b] These results clearly indicate that 2,3-QD enzymes have surprising variability in metal cofactor selectivity and structural flexibility for the metal-cofactor, and the catalytic activity of the enzymes are largely influenced by the metal ions.[5,6] The metal ion may control the orientation of the bound substrates, modulate the reduction potential of the bound substrate,[4] and provide electrostatic stabilization of the intermediates.[6b] However, little is known about the precise roles of metal ion and the carboxylate group as well as the catalytic mechanism of the individual enzymatic systems from the different origins. Similar phenomenon are also found in other enzyme systems such as ARD (Acireductone dioxygenase) (Fe, Ni, Co, Mn, and Mg)[7a] and extra-diol catechol dioxygenase (Fe, Co, and Mn).[7b] The metal diversity among the various enzymes for catalysis and the variability in metal cofactor selectivity in the same enzyme are a very interesting and poorly understood feature and will be a topic of further study.

There have been reported several biomimetic studies of 2,3-QD,[8−14] most of which, however, dealt with copper(II) complexes with polyamine supporting ligands.[8,9a,10] In those studies, little attention has been paid to the role of active site carboxylate (Glu). To the best of our knowledge, there are only two examples demonstrating that addition of excess free carboxylate to *N*-chelating ES-model complexes $[Cu^{II}(fla)(idpa)]ClO_4$ (idpa: 3,3′-iminobis(*N*,*N*-dimethylpropylamine)[9a] and $[Fe^{III}(fla)(salen)]$ ($salenH_2$: 1,6-bis-(2-hydroxyphenyl)-2,5-diaza-hexa-1,5-diene)[9b] accelerates the dioxygenation of the bound substrate flavonolate. The additional coordination by an exogenous carboxylate coligand may displace the carbonyl oxygen atom of the bidentate chelating flavonolate to monodentate ligand, enhancing the reactivity toward molecular oxygen. Two types of the model ligands having a carboxylate group have also been reported, $[Cu^{II}LCl]$ (L: 1-benzyl-4-acetato-1,4,7-triazacyclononane),[10a] $[Cu^{II}(BPEA)Obs]$ (BPEA: *N*,*N*-bis(2-pyridylmethyl)amino-2-ethanoate, Obs: *O*-benzoylsalicylic acid),[10b] as a resting enzyme and an enzyme−product (EP) complex model, respectively. However, no effect of the ligand carboxylate group on the reactivity was observed, and they required higher temperature (100 °C) to induce oxidative degradation of the substrate.

With respect to other transition-metal 2,3-QD model complexes, only a few examples have been reported such as $[Mn^{II}(fla)_2(py)_2]$,[11] $[Fe^{III}(4'\text{-MeOfla})_3]$,[11] $[Fe^{III}(fla)(salen)]$,[9b] $[Co^{III}(fla)(salen)]$,[12] $[(6\text{-}Ph_2TPA)M^{II}(fla)]X$ (M = Mn, Fe, Co, Ni, Cu, Zn; X: OTf^- or ClO_4^-; 6-Ph_2TPA: *N*,*N*-bis((6-phenyl-2-pyridyl)methyl)-*N*-((2-pyridyl)methyl)amine),[13a,b] and $[Zn^{II}(fla)(idpa)]ClO_4$,[14] among which $[(6\text{-}Ph_2TPA)M^{II}(fla)]X$ is the only example containing a series of divalent first row M^{II} ions. However, no reactivity study has been done on these model complexes.[13a]

While our manuscript was under review and revision (submitted April 19, 2013), a series of the ES models of 2,3-QD supported by a ligand having a carboxylate group $[M(fla)(L^1)]$ (M = Mn, Fe, Co, Ni, Cu; L^1: *N*-propanoate-*N*,*N*-bis(2-pyridylmethyl)amine) have been reported by Kaizer's group (received on May 23, 2013).[13c] The structure of the model ligand is very similar to that of ours, both of them are a *N*,*N*-bis(2-pyridylmethyl)amine N3O donor set ligands while another side arm is different. Kaizer's ligand has a *N*-propanoate side arm but ours has a *N*-benzonate side arm. The dioxygenation reactivity of the Kaizer's complexes (at 80 °C) are lower than ours (at 70 °C).

In order to get insights into the effects of metal ions as well as the carboxylate group on the chemical functions of 2,3-QD, we herein synthesized a series of M^{II}-flavonolate complexes supported by the carboxylate ligand L^- $[M^{II}L(fla)]$ (**LH**: 2-{[bis(pyridin-2-ylmethyl)amino]methyl}benzoic acid (Figure 1), fla: flavonolate, M = Mn (**1**), Fe (**2**), Co (**3**), Ni (**4**), Cu (**5**), and Zn (**6**)) as structural and functional models of ES-complexes of various metal(II)-containing 2,3-QD. The structure, physicochemical properties, redox properties, and reactivity toward molecular oxygen have been examined in detail.

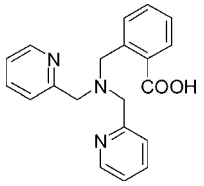

Figure 1. Structure of ligand **LH**.

EXPERIMENTAL SECTION

General and Physical Methods. All chemicals used in this study except the ligand and the complexes were commercial products of the highest available purity and were further purified by the standard method,[15] if necessary. FT-IR spectra were recorded with a Nicolet 6700 spectrophotometer. UV−vis spectra were measured using an Agilent Technologies HP8453 diode array spectrophotometer. ESI-MS (electrospray ionization mass spectra) measurements were performed on a PE SCIEX API 150EX or an Agilent Technologies HP1100LC-MSD, and the sample was prepared by adding a little amount of HOAc or $NH_3 \cdot H_2O$, if necessary. ^1H NMR spectra were recorded on a JEOL FT-NMR Lambda 300WB and 400WB or Bruker 400WB. EPR spectra were obtained on a Bruker MEX-Plus or Bruker A200 spectrometer fitted with a liquid helium cooled probe. The spectra of the complexes (2 or 4 mM in 0.5 mL DMF) were recorded at −150 °C for Cu^{II}-complex and −173 °C for Mn^{II}-, Fe^{II}-, and Co^{II}-complexes, about 20 mW microwave powers and about 9.40 GHz. The sample was put into a nitric acid washed quartz EPR tube and was frozen in liquid nitrogen. The data were simulated with WINEPR software. Cyclic voltammetry

dx.doi.org/10.1021/ic400972k | *Inorg. Chem.* 2013, 52, 10936−10948

data was collected using a CHI620b system. All CV data were obtained under N_2 in DMF with a complex concentration of 2 mM and $KClO_4$ (0.5 M) as the supporting electrolyte. The scan rate was 50 mV s^{-1}. The experimental setup consisted of a glassy carbon working electrode, an SCE reference electrode, and a platinum wire auxiliary electrode. All potentials are reported versus SCE. The organic reaction products were analyzed by HPLC-MS and ^{1}H NMR. HPLC-MS measurements were performed on a Thermo Fisher Scientific LTQ Orbitrap XL HPLC-MS. The production of the gas product CO during dioxygenation reaction was detected by online CO_x analyzer (SICK-MAIHAK-S710, Germany).

X-ray Crystallography. The single crystals were mounted on a glass capillary. Data of X-ray diffraction were collected by a Rigaku RAXIS-RAPID imaging plate two-dimensional area detector using graphite-monochromated Mo Kα radiation (λ = 0.71075 Å) to $2\theta_{max}$ of 55.0°. The crystallographic calculations were performed using the Crystal Structure software package of the Rigaku Corporation and Molecular Structure Corporation for **2**[38] and **3**[39] and SHELXTL 97 for **4**.[40] All non-hydrogen atoms and hydrogen atoms were refined anisotropically and isotropically, respectively. Since the disordered H_2O solvent molecules in **4** could not be unambiguously modeled, the Platon Squeeze option was utilized to remove all of them.[41] Squeeze indicates 2 solvent regions in the cell corresponding to about 86 electrons/cell or approximately 2 H_2O molecules per formula.

Kinetic Measurements. *[M^{II}L(fla)] Dependence.* The reactions of the complexes [M^{II}L(fla)] (M = Mn, Fe, Co, Ni, Cu, and Zn) with O_2 were carried out in a 10 mm path length UV−vis cell that was held in a Unisoku thermostatted cell holder USP-203 (a desired temperature can be fixed within ±0.5 °C). After the deaerated solution (3 mL) of [M^{II}L(fla)] (0.8−2.0 × 10^{-4} M) in the cell was kept at a desired temperature (70 °C) for several minutes, dry dioxygen gas was continuously supplied by gentle bubbling from a thin needle. The time courses of the reactions were followed by monitoring the absorption change at a λ_{max} due to the $\pi \rightarrow \pi^*$ transition of the coordinated flavonolate. The initial concentrations of [M^{II}L(fla)] were determined by using the ε value at the λ_{max} of each complex (see Table 3).

O_2 Dependence. After the deaerated solvent DMF (58 mL) in a thermostatted reaction vessel was kept at a desired temperature (30−80 ± 0.5 °C) and a constant dioxygen pressure through a manometer for several minutes, the deaerated solution of [M^{II}L(fla)] (3 mM in 2 mL DMF) was added. The reaction mixture was then taken by syringe periodically (ca. every 2 min), and the time courses of the reactions were followed by monitoring the absorption change at a λ_{max} due to the $\pi \rightarrow \pi^*$ transition of the coordinated flavonolate. The O_2 concentrations were calculated from literature data[16] taking into account the partial pressure of DMF[17] and assuming the validity of Dalton's law.

Determination of the Activation Parameters. The activation parameters for the degradation of [M^{II}L(fla)] were obtained from an Eyring plot (Table 4, Supporting Information Figures S4 and S12) with [M^{II}L(fla)] (0.1 × 10^{-4} M) in the temperature range of 55−95 °C. The experiments procedures were similar to kinetic study described above.

Reaction Product Analysis. *By HPLC-MS.* After the deaerated DMF solution (2 mL) of [M^{II}L(fla)] (1.0 × 10^{-3} M) in the cell was kept at 70 °C for several minutes, dry dioxygen gas was continuously supplied by gentle bubbling from a thin needle for 8 h. After the reaction, the mixture was concentrated by evaporation, and the remaining residue was dissolved in 1.9 mL MeOH. *o*-Methylbenzoic acid (10 mM in 100 μL MeOH solution, total 0.5 mM in 2.0 mL solution) was added to the above solution as an internal standard, and the reaction products were analyzed with a Thermo Fisher Scientific LTQ Orbitrap XL HPLC-MS with an online UV−vis detector (λ: 210 nm). A Hypersil GOLD C18 column (Thermo Fisher Scientific 150 mm × 2.1 mm, 5 μm) was used for the HPLC analysis at room temperature with a mobile phase (MeOH and 5 mM HOAc−NH_4OAc buffer (pH = 3.00)) with some gradient at a constant flow rate of 0.8 mL min^{-1}. The yields of the reaction products were calculated by using the standard calibration curve.

By ^{1}H NMR. The [Fe^{II}L(fla)] (1.0 × 10^{-3} M in 200 mL DMF) solution was reacted with O_2 at 100 °C for 1 day. The reaction mixture was evaporated, esterificated by CH_3OH in the presence of H_2SO_4, and then extracted with CH_2Cl_2. The products were separated by using silica gel column chromatography and analyzed by ^{1}H NMR (in $CDCl_3$).

CO Analysis. A homemade reactor was linked with a pure N_2 and an O_2 gas tank and an online CO_x analyzer. Dry N_2 gas (100 mL min^{-1}) was continuously supplied by bubbling to a deaerated DMF solution (30 mL) of [Fe^{II}L(fla)] (1.0 × 10^{-3} M) in the reactor for 30 min to degas the CO_2, CO, and O_2 in solution, reactor, and all of the system lines. The solution was kept at 70 °C for several minutes until the CO and CO_2 concentrations were lower than 1 and 9 ppm, respectively. Then dry O_2 and N_2 gas (30:70) were continuously supplied by bubbling, the analyses were started, and the online CO and CO_2 gas concentrations were recorded for 6.5 h. The reaction was monitored at 70 °C during the initial 50 min. After 50 min, the reaction became very slow, so we increased the reaction temperature to 100 °C. After 342 min, the CO concentration was lower than 1 ppm, we stopped the detection of CO. The total CO concentration was integrated for the whole reaction time.

Synthesis of the Model Complexes. Ligand **LH** was prepared according to the reported procedures.[18]

*[Mn^{II}L(fla)]·H_2O (**1**).* A dry CH_2Cl_2 (1.0 mL) solution of flavonol (72.2 mg, 0.3 mmol) was added dropwise to a dry MeOH/acetonitrile (3:1) solution (4.0 mL) of $Mn(OAc)_2·4H_2O$ (74.7 mg, 0.3 mmol) at room temperature under Ar. After stirring for 1 day, the solvent was removed by evaporation, and the resulting mixture was dissolved in CH_2Cl_2 (2.0 mL). A dry CH_2Cl_2 solution (1.0 mL) containing ligand **LH** (100.0 mg, 0.3 mmol) was added dropwise to the above solution, then the mixture was stirred for another 1 day under Ar. The [Mn^{II}L(fla)] was isolated as yellow-green powder by filtration. Light yellow thin crystals were obtained by slow diffusion of hexane into the dichloromethane solution of the complex at room temperature (96.0 mg, 51%). ESI-MS: *m*/*z* (pos.) = 625.3 ([Mn^{II}L(fla)]H^+), 647.3 ([Mn^{II}L(fla)]Na^+), 663.2 ([Mn^{II}L(fla)]K^+) (main peak). Anal. calc for $C_{35}H_{29}MnN_3O_6$ (642.56): C, 65.42; H, 4.55; N, 6.54. Found: C, 65.23; H, 4.63; N, 6.89. FT-IR (solid sample: KBr, cm^{-1}): 3488 (m), 1609 (s), 1562 (s), 1480 (w), 1444 (w), 1389 (s), 1105 (m), 764 (m). FT-IR (solution sample: in ethanol, cm^{-1}): 3331 (m), 1600 (w), 1583 (s), 1560 (s), 1481 (w), 1444 (w), 1385 (s), 1125 (w), 759 (m).

*[Fe^{II}L(fla)]·H_2O (**2**).* This compound was synthesized by a similar manner as for the synthesis of [Mn^{II}L(fla)] except using $Fe(OAc)_2$ (54.9 mg, 0.3 mmol) instead of $Mn(OAc)_2·4H_2O$. The [Fe^{II}L(fla)] was isolated as dark red powder by filtration. Dark red single crystals suitable for X-ray crystallographic analysis were obtained from the filtrate by slow evaporation of the solvent (95.7 mg, 51%). ESI-MS: *m*/*z* (pos.) = 626.2 ([Fe^{II}L(fla)]H^+) (main peak), 648.2 ([Fe^{II}L(fla)]Na^+). Anal. calc for $C_{35}H_{29}FeN_3O_6$ (643.48): C, 65.33; H, 4.54; N, 6.53. Found: C, 65.50; H, 4.67; N, 6.32. FT-IR (solid sample: KBr, cm^{-1}): 3374 (m), 1609 (m), 1589 (m), 1544 (s), 1504 (w), 1488 (s), 1440 (w), 1416 (s), 1356 (s), 1321 (w), 1213 (m), 753 (m). FT-IR (solution sample: in ethanol, cm^{-1}): 3331 (m), 1613 (m), 1588 (m), 1545 (s), 1504 (w), 1489 (s), 1440 (w), 1417 (s), 1355 (s), 1321 (w), 1215 (s), 754 (m).

*[Co^{II}L(fla)]·CH_3OH (**3**).* This compound was synthesized by a similar manner as for the synthesis of [Mn^{II}L(fla)] except using the corresponding $Co(OAc)_2·4H_2O$ (75.5 mg, 0.3 mmol) instead of $Mn(OAc)_2·4H_2O$. The complex was isolated as reddish-yellow powder. Wine red single crystals suitable for X-ray crystallographic analysis were obtained by slow diffusion of hexane into the dichloromethane solution of the complex at room temperature (88.3 mg, 47%). ESI-MS: *m*/*z* (pos.) = 629.0 ([Co^{II}L(fla)]H^+), 651.2 ([Co^{II}L(fla)]Na^+), 667.2 ([Co^{II}L(fla)]K^+) (main peak). Anal. calc for $C_{36}H_{31}CoN_3O_6$ (660.57): C, 65.46; H, 4.73; N, 6.36. Found: C, 65.63; H, 4.53; N, 6.67. FT-IR (solid sample: KBr, cm^{-1}): 3449 (m), 1610 (m), 1592 (s), 1561 (s), 1481 (w), 1439 (w), 1412 (s), 1377 (s), 1217 (m), 760 (m). FT-IR (solution sample: in ethanol, cm^{-1}): 3331 (m), 1605 (m), 1588 (s), 1553 (s), 1481 (m), 1435 (w), 1414 (w), 1378 (s), 1219 (w), 768 (w).

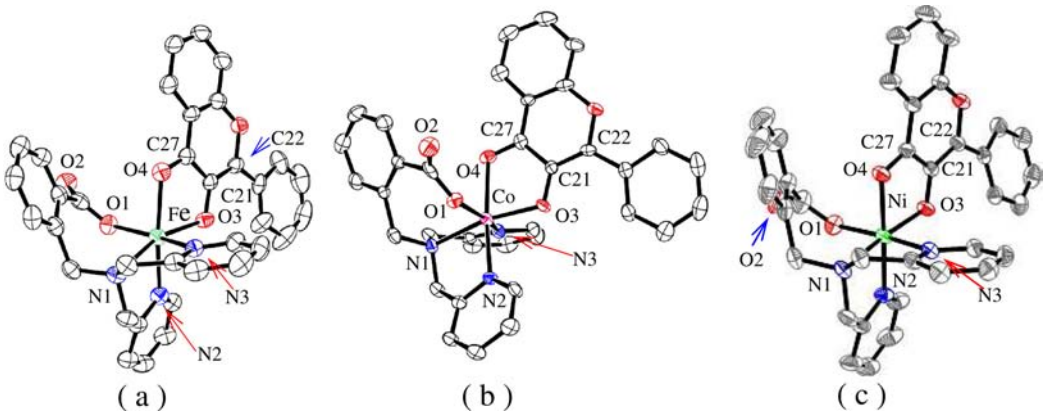

Figure 2. ORTEP representation of (a) $[Fe^{II}L(fla)]\cdot H_2O$ (**2**), (b) $[Co^{II}L(fla)]\cdot CH_3OH$ (**3**), and (c) $[Ni^{II}L(fla)]$ (**4**). Ellipsoids are shown at the 50% probability level. Hydrogen atoms and solvents molecules are omitted for clarity.

*$[Ni^{II}L(fla)]\cdot 2H_2O$ (**4**).* This compound was synthesized by a similar manner as for the synthesis of $[Mn^{II}L(fla)]$ except using $Ni(OAc)_2\cdot 4H_2O$ (74.7 mg, 0.3 mmol) instead of $Mn(OAc)_2\cdot 4H_2O$. The complex was isolated as yellow-green powder. Yellow-green single crystals suitable for X-ray crystallographic analysis were obtained by slow diffusion of ether into the dichloromethane solution of the complex at room temperature (109.2 mg, 58%). ESI-MS: *m*/*z* (pos.) = 628.2 ($[Ni^{II}L(fla)]H^+$), 650.3 ($[Ni^{II}L(fla)]Na^+$) (main peak), 666.2 ($[Ni^{II}L(fla)]K^+$). Anal. calc for $C_{35}H_{31}N_3NiO_7$ (664.33): C, 63.28; H, 4.70; N, 6.33. Found: C, 63.22; H, 4.77; N, 6.26. FT-IR (solid sample: KBr, cm^{-1}): 3438 (m), 1605 (s), 1591 (s), 1553 (s), 1479 (m), 1417 (m), 1368 (s), 1224 (m), 761 (m). FT-IR (solution sample: in ethanol, cm^{-1}): 3331 (m), 1605 (w), 1587 (s), 1548 (s), 1484 (m), 1417 (m), 1397 (s), 1221 (m), 754 (w).

*$[Cu^{II}L(fla)]\cdot 3CH_3OH$ (**5**).* This compound was synthesized by a similar manner as for the synthesis of $[Mn^{II}L(fla)]$ except using $Cu(OAc)_2\cdot H_2O$ (60.5 mg, 0.3 mmol) instead of $Mn(OAc)_2\cdot 4H_2O$. The complex was isolated as dark green powder. Pure sample crystals were obtained by slow diffusion of hexane into the dichloromethane solution of the complex at room temperature (59.5 mg, 31%). ESI-MS: *m*/*z* (pos.) = 633.3 ($[Cu^{II}L(fla)]H^+$). Anal. calc for $C_{38}H_{39}CuN_3O_8$ (729.28): C, 62.58; H, 5.39; N, 5.76. Found: C, 62.74; H, 5.65; N, 5.40. FT-IR (solid sample: KBr, cm^{-1}): 3447 (m), 1609 (s), 1554 (s), 1487 (m), 1446 (m), 1384 (s), 1213 (m), 759 (m). FT-IR (solution sample: in ethanol, cm^{-1}): 3331 (m), 1612 (w), 1589 (m), 1538 (s), 1490 (s), 1441 (w), 1420 (s), 1357 (s), 1316 (w), 1215 (m), 750 (w).

*$[Zn^{II}L(fla)]\cdot 3CH_3OH$ (**6**).* This compound was synthesized by a similar manner as for the synthesis of $[Mn^{II}L(fla)]$ except using $Zn(OAc)_2\cdot 2H_2O$ (66.6 mg, 0.3 mmol) instead of $Mn(OAc)_2\cdot 4H_2O$. The complex was isolated as bright yellow powder (165.5 mg, 75%). ESI-MS: *m*/*z* (pos.) = 634.1 ($[Zn^{II}L(fla)]H^+$). Anal. calc for $C_{38}H_{39}ZnN_3O_8$ (731.12): C, 62.43; H, 5.38; N, 5.75. Found: C, 62.65; H, 5.56; N, 5.52. FT-IR (solid sample: KBr, cm^{-1}): 3427 (m), 1610 (w), 1590 (s), 1563 (s), 1484 (m), 1441 (s), 1410 (s), 1383 (s), 1217 (m), 759 (s). FT-IR (solution sample: in ethanol, cm^{-1}): 3331 (m), 1610 (w), 1591 (s), 1558 (s), 1485 (m), 1442 (m), 1409 (m), 1381 (s), 1217 (w), 757 (s). ^1H NMR ($CDCl_3$, 400 MHz): δ (ppm) 8.82 (d, J = 2.4 Hz, 2 H), 8.61 (t, J = 2.0 Hz, 2 H), 8.05 (d, J = 6.0 Hz, 1 H), 7.91 (d, J = 6.0 Hz, 1 H), 7.66 (d, J = 8.8 Hz, 2 H), 7.20–7.60 (m, 11 H), 7.06 (t, J = 4.8 Hz, 1 H), 6.97 (d, J = 8.0 Hz, 1 H), 3.92 (s, 4 H), 3.48 (s, 2 H).

RESULTS AND DISCUSSION

Synthesis and Structural Characterization. All the model complexes $[M^{II}L(fla)]$ (M = Mn (**1**), Fe (**2**), Co (**3**), Ni (**4**), Cu (**5**), and Zn(**6**)) were synthesized by treating the neutral ligand **LH**, flavonol (flaH), and $M^{II}(OAc)_2$ under Ar without adding any base. In these cases, acetate ions (OAc^-) of $M^{II}(OAc)_2$ may act as a proton acceptor both from **LH** and flaH in the reaction. All the complexes are relatively stable under air in the solid state but readily react with O_2 in solution (see below). Single crystals of complexes $[Fe^{II}L(fla)]\cdot H_2O$ (**2**), $[Co^{II}L(fla)]\cdot CH_3OH$ (**3**), and $[Ni^{II}L(fla)]$ (**4**) suitable for X-ray crystallographic analysis were successfully obtained as shown in Figure 2a, b, and c, respectively. A summary of the crystallographic data is shown in Table 1 together with the selected bond lengths and angles listed in Table 2. The Fe^{II}- and Co^{II}-complexes crystallize in the orthorhombic system and *Pbca* space group, while the Ni^{II}-complex crystallizes in the monoclinic system and *P*2(*1*)/*c* space group. These ternary complexes exhibit a very similar structure, where the metal center of each complex has a distorted octahedral geometry involving two oxygen atoms of fla^- (O(3): 3-hydroxylate and O(4): 4-carbonyl), one oxygen atom of ligand L^- (O(1): benzoate) and three nitrogen atoms of ligand L^-, where O(4) and N(2) (one of the pyridine nitrogen atoms) occupy the axial positions.

The bond lengths of M–O(1) (benzoate of L^-) are 2.0256(18) Å for **2**, 2.0165(14) Å for **3**, and 2.076(2) Å for **4**, respectively, which are slightly shorter than those of the resting Fe^{II}- and Cu^{II}-containing 2,3-QD (2.10 Å)[2,5a] and much shorter than that of the ES adduct of the Cu^{II}-containing 2,3-QD (2.28 Å),[3] but longer than that of $[Fe^{III}(fla)(L^1)]ClO_4$ (1.909(5) Å).[13c] The bond lengths of Fe–O(3) and Fe–O(4) (oxygen atoms of fla^-) in **2** are 2.0297(16) and 2.1893(17) Å, respectively, which are longer than those of the reported Fe^{III}-flavonolate complexes $[Fe^{III}(fla)(L^1)]ClO_4$ (1.912(5) and 2.100(5) Å),[13c] $[Fe^{III}(4'\text{-MeOfla})_3]$ (1.955(7) and 2.109(8) Å),[11a] $[Fe^{III}(fla)(salen)]$ (1.955(4) and 2.139(4) Å),[9b] $[Fe^{III}(fla)_2Cl(MeOH)]$ (1.958(12) and 2.127(63) Å),[19] and $[(6\text{-}Ph_2TPAFe^{III}(fla))_2(\mu\text{-}O)](ClO_4)_2$ (1.9683(64) and 2.1257(15) Å).[13a] The average Fe–N bond length is 2.23 Å, which is also slightly longer than those of $[Fe^{III}(fla)(L^1)]ClO_4$ (2.15 Å)[13c] and $[(6\text{-}Ph_2TPAFe^{III}(fla))_2(\mu\text{-}O)](ClO_4)_2$ (2.21 Å).[13a] These results indicate that the oxidation state of Fe ion is +2 in **2**, which is in good agreement with the calculated valence[20] of the Fe ion (2.02) and the EPR results (silent) described below. The difference $[\Delta d(Fe-O)]$ between Fe–O(3) and Fe–O(4) is 0.16 Å, which is similar to those of $[Fe^{III}(fla)(L^1)]ClO_4$ (0.19 Å),[13c] $[Fe^{III}(4'\text{-MeOfla})_3]$ (0.15 Å),[11a] $[Fe^{III}(fla)(salen)]$ (0.18 Å),[9b] $[Fe^{III}(fla)_2Cl(MeOH)]$ (0.17 Å),[19] and $[(6\text{-}Ph_2TPAFe^{III}(fla))_2(\mu\text{-}O)](ClO_4)_2$ (0.17 Å).[13a]

dx.doi.org/10.1021/ic400972k | *Inorg. Chem.* 2013, 52, 10936–10948

Table 1. Summary of X-ray Data Collection and Refinement

	[Fe^{II}L(fla)]·H_2O (**2**)	[Co^{II}L(fla)]·CH_3OH (**3**)	[Ni^{II}L(fla)] (**4**)
empirical formula	$C_{35}H_{29}FeN_3O_6$	$C_{36}H_{31}CoN_3O_6$	$C_{35}H_{27}N_3NiO_5$
M_r	643.48	660.57	628.31
crystal system	orthorhombic	orthorhombic	monoclinic
space group	*Pbca*	*Pbca*	*P*2(1)/*c*
a/Å	9.560(4)	9.690(3)	11.3376(5)
b/Å	20.519(7)	21.045(7)	32.5833(12)
c/Å	30.232(9)	30.112(13)	8.8492(4)
α/deg	90	90	90
β/deg	90	90	101.996(3)
γ/deg	90	90	90
V/Å^3	5931(4)	6140(4)	3197.7(2)
Z	8	8	4
d_{calcd}/g cm^{-3}	1.437	1.427	1.305
T/K	153	163	296(2)
crystal habit	prism	prism	block
color	dark red	wine red	yellow-green
crystal size (mm^3)	0.20 × 0.20 × 0.050	0.40 × 0.20 × 0.10	0.30 × 0.15 × 0.10
μ/mm^{-1}	0.561	0.606	0.652
$2\theta_{max}$/deg	54.96	54.96	52.00
completeness to θ (%)	99.9	99.9	100
reflections collected	53872	55197	23266
independent reflections	6803	7027	6274
R_{int}	0.0590	0.0500	0.0414
variable parameters	433	445	397
$R1^a$/w$R2^b$	0.0417/0.0835	0.0286/0.0368	0.0435/0.1078
goodness-of-fit on F^2	1.048	1.015	1.033
$\Delta\rho_{max/min}$/e Å^{-3}	1.070/−0.606	0.86/−0.34	0.259/−0.285

$^a R1 = \sum(||F_o| - |F_c||)/\sum|F_o|$. $^b wR2 = [\sum w(F_o^2 - F_c^2)^2/\sum w(F_o^2)^2]^{1/2}$, where $w = 1/[\sigma^2(F_o^2) + (aP)^2 + bP]$.

The Co−O(3) and Co−O(4) distances in **3** are 1.9993(14) and 2.1797(14) Å, respectively, which are close to that of [Co^{II}(6-Ph_2TPA)(fla)]ClO_4 (1.956(2) and 2.172(2) Å, respectively).[13a] The difference [Δd(Co−O)] between Co−O(3) and Co−O(4) is 0.18 Å, which is also similar to that of **2** and [Co^{II}(6-Ph_2TPA)(fla)]ClO_4 (0.22 Å).[13a] The average Co−N distance is 2.16 Å, which is close to those of **2** and [Co^{II}(6-Ph_2TPA)(fla)]ClO_4 (2.22 Å).[13a] These results indicate that the oxidation state of Co ion in **3** is also +2, which is consistent with the calculated valence[20] of the Co ion (1.86) and the EPR results described below.

The Ni−O(3) and Ni−O(4) bond lengths in **4** are 2.0145(16) and 2.0604(16) Å, respectively, which are close to those of [Ni^{II}(6-Ph_2TPA)(fla)]ClO_4 (1.996(2) and 2.031(2) Å, respectively).[13a] The difference [Δd(Ni−O)] between Ni−O(3) and Ni−O(4) is 0.046 Å, which is shorter than those of **2** and **3** and similar to that of [Ni^{II}(6-Ph_2TPA)(fla)]ClO_4 (0.035 Å).[13a] The average Ni−N bond length is 2.09 Å, which is close to those of **2**, **3**, and [Ni^{II}(6-Ph_2TPA)(fla)]ClO_4 (2.16 Å).[13a]

The C(21)−O(3) bond lengths (corresponding to C(3)—O(3-hydroxylate) of the enzymatic substrate, Scheme 1) are 1.316(3) Å for **2**, 1.313(2) Å for **3**, and 1.311(3) Å for **4**, respectively, which are slightly contracted relative to free flavonol (flaH) (1.357(3) Å).[21] The C(27)—O(4) bond lengths (corresponding to C(4)=O(4-carbonyl) of the enzymatic substrate, Scheme 1) are 1.261(3) Å for **2**, 1.259(2) Å for **3**, and 1.259(3) Å for **4**, respectively, which, on the other hand, are slightly elongated relative to free flavonol (1.232(3) Å).[21] The C(21)=C(22) bond lengths (corresponding to C(2)=C(3) of the enzymatic substrate, Scheme 1) are 1.372(3) Å for **2**, 1.376(2) Å for **3**, and 1.381(3) Å for **4**, respectively, which are slightly elongated relative to free flavonol (1.363(4) Å),[21] indicating that the C=C bond is elongated by the metal coordination, which may promote the C(21)=C(22) bond cleavage during reaction with O_2 described below (Scheme 3). These results indicate that the C(22) atom (corresponding to C(2) of the enzymatic substrate, Scheme 1) increases sp^3 character by pyramidalization as found in the ES adduct of Cu^{II}-containing 2,3-QD from *A. japonicas*.[3] It has been proposed that such a structural feature stabilizes substrate radical produced from the reaction with O_2.[3]

Table 2. Selected Bond Lengths (Å) and Bond Angles (deg) for the Complexes

	[Fe^{II}L(fla)]·H_2O (**2**)	[Co^{II}L(fla)]·CH_3OH (**3**)	[Ni^{II}L(fla)] (**4**)
M(1)−O(1)	2.0256(18)	2.0165(14)	2.076(2)
M(1)−O(3)	2.0297(16)	1.9993(14)	2.0145(16)
M(1)−O(4)	2.1893(17)	2.1797(14)	2.0604(16)
M(1)−N(1)	2.297(2)	2.2173(17)	2.114(2)
M(1)−N(2)	2.191(2)	2.1360(15)	2.053(2)
M(1)−N(3)	2.189(3)	2.1371(17)	2.095(2)
O(3)−C(21)	1.316(3)	1.313(2)	1.311(3)
O(4)−C(27)	1.261(3)	1.259(2)	1.259(3)
C(21)−C(22)	1.372(3)	1.376(2)	1.381(3)
O(1)−M(1)−O(3)	108.78(7)	103.08(5)	94.62(7)
O(1)−M(1)−O(4)	87.74(7)	85.22(5)	93.11(8)
O(3)−M(1)−O(4)	78.02(7)	79.30(5)	81.90(6)
O(1)−M(1)−N(1)	86.64(7)	88.07(6)	92.29(8)
O(1)−M(1)−N(2)	89.53(7)	88.48(6)	84.59(8)
O(1)−M(1)−N(3)	155.61(7)	157.83(6)	171.12(8)
O(3)−M(1)−N(1)	160.81(7)	166.52(6)	173.05(8)
O(3)−M(1)−N(2)	90.59(7)	93.22(6)	97.98(8)
O(3)−M(1)−N(3)	90.59(7)	95.30(6)	93.91(8)
O(4)−M(1)−N(1)	114.93(7)	109.55(5)	98.41(7)
O(4)−M(1)−N(2)	166.72(7)	168.84(6)	177.69(8)
O(4)−M(1)−N(3)	87.23(7)	86.14(6)	85.65(8)
N(1)−M(1)−N(2)	77.85(7)	79.37(6)	82.00(8)
N(1)−M(1)−N(3)	73.96(8)	75.68(6)	79.21(8)
N(2)−M(1)−N(3)	100.40(8)	102.91(6)	96.67(8)

There are only four structurally characterized iron(III)−flavonolate complexes [Fe^{III}(fla)(L^1)]ClO_4,[13c] [Fe^{III}(4′-MeO-fla)$_3$],[11a] [Fe^{III}(fla)(salen)],[9b] and [Fe^{III}(fla)$_2$Cl(MeOH)],[19] but their oxidation state or/and structures are very different from that of the ES adduct of the Fe^{II}-containing 2,3-QD. [Fe^{II}(fla)(L^1)][13c] and [(6-Ph_2TPA)Fe^{II}(fla)]ClO_4[13a] are the only two examples of iron(II)−flavonolate complexes mimicking the reduced state of Fe^{II}-containing 2,3-QD. However, they were not structurally characterized, and the dioxygenation reactivity of [Fe^{II}(fla)(L^1)] was lower and required higher temperature. [(6-Ph_2TPA)Fe^{II}(fla)]ClO_4 reacted with O_2 to give a (μ-oxo)diiron(III) complex [(6-Ph_2TPAFe^{III}(fla))$_2$(μ-O)]$(ClO_4)_2$, and no enzyme-like dioxygenation reactivity (dioxygenation of the bound flavonolate) study has been done on this complex. There is only one structurally

dx.doi.org/10.1021/ic400972k | *Inorg. Chem.* 2013, 52, 10936−10948

Table 3. Summary of Spectroscopic and CV Data for the Complexes

		[Mn^{II}L(fla)] (1)	[Fe^{II}L(fla)] (2)	[Co^{II}L(fla)] (3)	[Ni^{II}L(fla)] (4)	[Cu^{II}L(fla)] (5)	[Zn^{II}L(fla)] (6)
				FT-IR			
ν(CO)/cm^{-1}		1562	1561	1561	1553	1554	1563
$\nu_{as}(CO_2)$/cm^{-1}		1609	1589	1592	1591	1609	1610
$\nu_{s}(CO_2)$/cm^{-1}		1389	1356	1377	1368	1384	1383
$\Delta\nu$/cm^{-1}		220	233	215	223	225	227
UV−vis		275 (14347)	275 (13516)	278 (16231)	278 (15650)	275 (23253)	278 (14356)
λ/nm (ε/M^{-1} cm^{-1})		422 (10695)	398 (9384)	417 (13281)	440 (15184)	423 (10205)	417 (9909)
			486 (2250)	510 (548)	567 (47)	658 (212)	
			570 (371)	607 (247)	775 (4.4)		
					972 (24)		
ESI-MS m/z		663.2 ([Mn^{II}L(fla)]K^+)	626.2 ([Fe^{II}L(fla)] H^+)	667.2 ([Co^{II}L(fla)]K^+)	650.3 ([Ni^{II}L(fla)]Na^+)	633.3 ([Cu^{II}L(fla)]H^+)	634.1 ([Zn^{II}L(fla)]H^+)
EPR		g: 2.01	silent	g: 5.60		$g_{//}$: 2.25	
		A: 95 G		g: 2.25		$g_{\perp}$: 2.06	
		g: 5.62				$A_{//}$: 159 G	
μ_{eff}/B.M.		5.94		4.13	3.12	1.99	
CV	$E_{1/2}$ (V)		−0.094	−0.062		−0.427	
	E_{pa} (V)	+0.469	+0.169	+0.396	+0.401	+0.243	+0.438
	E_{pc} (V)		+0.091	+0.216			
	$E_{1/2}$ (V)		+0.130	+0.306			

characterized example of the cobalt(II)−flavonolate complex [Co^{II}(6-Ph_2TPA)(fla)]ClO_4,[13a] but it only exhibits ligand exchange reactivity. No enzyme-like dioxygenation reactivity study is reported on this complex. There are two structurally characterized examples of the nickel(II)−flavonolate complexes [$Ni^{II}(Py)_2(fla)_2$][22] and [Ni^{II}(6-Ph_2TPA)(fla)]ClO_4,[13a] but no enzyme-like dioxygenation reactivity study on these complexes is reported. Thus, our complexes [Fe^{II}L(fla)]·H_2O (**2**), [Co^{II}L(fla)]·CH_3OH (**3**), and [Ni^{II}L(fla)] (**4**) are the first examples of structurally characterized M^{II}-flavonolate complexes, which exhibit an enzyme-like dioxygenation reactivity as demonstrated below.

Spectroscopic and Redox Properties of the Complexes. *Infrared Spectroscopy.* The FT-IR spectra of the solid samples (Table 3, Supporting Information Figure S1-C for **2**) show a C═O stretching vibration ν(C═O) of the coordinated carbonyl group of fla$^-$ around 1560 cm^{-1}, which is lower by 40−60 cm^{-1} as compared with that of free flavonol (1602 cm^{-1}). A similar phenomenon found in other flavonolate complexes so far has been reported.[8−14] The asymmetric $\nu_{as}(COO^-)$ and symmetric $\nu_s(COO^-)$ stretching frequencies of the carboxylate group of L$^-$ in the complexes appear at ∼1600 and ∼1380 cm^{-1}, respectively, which are also lower as compared with those of free ligand **LH** (1696 and 1594 cm^{-1}, respectively). The difference between them ($\Delta\nu$ = $\nu_{as}(COO^-) - \nu_s(COO^-)$) is about 220 cm^{-1}, suggesting a monodentate carboxylate binding mode,[23,24] consistent with the X-ray structures shown in Figure 2.

In order to get insight into the solution structure of the complexes, FT-IR spectra of the complexes were also recorded in ethanol (Supporting Information Table S1, Figure S1-B for **2**). The solution spectrum of each complex is similar to that of the corresponding solid sample. The complexes also show a C═O stretching vibration ν(CO) of the coordinated carbonyl group of fla$^-$ at ∼1550 cm^{-1} and the asymmetric $\nu_{as}(COO^-)$ and symmetric $\nu_s(COO^-)$ stretching frequencies of the carboxylate group of L$^-$ at ∼1590 and ∼1380 cm^{-1}, respectively. The difference between them ($\Delta\nu$ = $\nu_{as}(COO^-) - \nu_s(COO^-)$) is about 210 cm^{-1}, also suggesting a monodentate carboxylate binding mode in solution.[23,24] These results clearly indicate that the complexes keep their mononuclear structures in solution, which is in agreement with other spectroscopic results such as ESI-MS, solution magnetic moment, solution EPR, and NMR described bellow.

UV−vis Spectroscopy. Complexes [M^{II}L(fla)] exhibit an intense absorption band at 398−440 nm (Mn: 422 nm (ε = 1.1 × 10^4 M^{-1} cm^{-1}), Fe: 398 nm (ε = 9.4 × 10^3 M^{-1} cm^{-1}) (Figure 4a red line), Co: 417 nm (ε = 1.3 × 10^4 M^{-1} cm^{-1}), Ni: 440 nm (ε = 1.5 × 10^4 M^{-1} cm^{-1}), Cu: 423 nm (ε = 1.0 × 10^4 M^{-1} cm^{-1}), Zn: 417 nm (ε = 9.9 × 10^3 M^{-1} cm^{-1}) Supporting Information Figure S2 and Table 3), which can be assigned to the $\pi \rightarrow \pi^*$ transition of the B ring (Scheme 1) of the coordinated flavonolate ligand.[25] The λ_{max} of our model complexes [M^{II}L(fla)] are blue-shifted by 3−17 nm as compared to those of [M^{II}(6-Ph_2TPA)(fla)]ClO_4 (Mn: 431 nm, Fe: 415 nm, Co: 422 nm, Ni: 443 nm, Cu: 428 nm, Zn: 420 nm),[13a] [M^{II}(fla)(L^1)] (Mn: 430 nm, Fe: 402 nm, Co: 423 nm, Ni: 450 nm, Cu: 432 nm),[13c] and other synthetic model complexes such as [Fe^{III}(fla)(salen)] (407 nm),[9b] [Fe^{III}(4′-MeOfla)$_3$] (411 nm),[11a] and [Mn^{II}(fla)$_2$(py)$_2$] (432 nm).[11a] The shift of the λ_{max} of [Fe^{II}L(fla)] (**2**) is especially larger (4−17 nm) than those of [Fe^{II}(6-Ph_2TPA)(fla)]ClO_4,[13a] [Fe^{III}($^-$a)-(salen)],[9b] and [Fe^{III}(4′-MeOfla)$_3$],[11a] due to the existing negative charge of the caboxylate group of our supporting ligand and lower charge (+2 relative to +3) and low spin state of Fe(II) ion (see below). The bands are blue-shifted relative to those of free flavonolate (458 nm for Me_4Nfla[13a] and 465 nm for Kfla[26]) about 20−50 nm and in the order of Ni < Cu < Mn < Co ∼ Zn < Fe, which is consistent with the order observed with [M^{II}(fla)(L^1)][13c] and [(6-Ph_2TPA)M^{II}(fla)]ClO_4,[13a] indicating that the degree of the blue-shift is markedly affected by the nature of the M(II) ion. The electron distribution of the coordinated substrate flavonolate may be altered by the nature of the M(II) ion via the "electronic bridge" conferred by C(21)═C(22) double bond (corresponding to C(2)═C(3) of the enzymatic substrate, Scheme 1) as found in the enzyme system.[6b] This tendency is similar to those seen in the enzymatic[2−6] and other synthetic model systems.[8−14] The Fe-,

dx.doi.org/10.1021/ic400972k | Inorg. Chem. 2013, 52, 10936−10948

Co-, Ni-, and Cu-complexes also exhibit one or two weak d−d absorption bands in the visible region (Table 3).

Our binary complex [Fe^{II}L(OAc)] (without fla^-) was very sensitive to air in solution, being easily auto-oxidized to form a μ-oxo dimer [LFe^{III}(μ-O)(μ-OAc)Fe^{III}L](OAc) (characterized by ESI-MS (m/z (pos.): 851.2 ([LFe^{III}(μ-O)(μ-OAc)Fe^{III}L]$^+$)) and single crystal X-ray diffraction, unpublished results). Our ternary complex [Fe^{II}L(fla)] (398 nm) was also very sensitive to air in solution, which could be oxidized to [Fe^{III}L(fla)]$^+$ (m/z (pos.): 625.2). In this case, however, no oxo or flavonolate bridged dimer was observed in the ESI-MS spectrum (Supporting Information Figure S3). When a [Fe^{II}L(fla)] solution was exposed to air or O_2, the band was shifted to 402 nm, which is similar to the Fe(III) analogue [Fe^{III}L(fla)](OAc) (**2A**) (406 nm) described bellow (Supporting Information Table S4, Figure S12a). The spectrum of [Fe^{II}L(fla)] (**2**) is very similar to those of [Fe^{II}(fla)(L^1)] (402 nm)[13c] and [Fe^{II}(6-Ph_2TPA)(fla)]ClO_4[13a] (also have a shoulder peak at near 500 nm), but different from that of the μ-oxo dimer [LFe^{III}(μ-O)(μ-OAc)Fe^{III}L](OAc) (317 and 484 nm). These results indicate that [Fe^{II}L(fla)] keeps a mononuclear structure in solution even after auto-oxidation, which is consistent with the solution FT-IR, ESI-MS, solution EPR, and solution magnetic moment results (see below).

ESI-MS Spectroscopy. The solution structures of the complexes were also examined by ESI-MS. The complexes exhibit a peak cluster as a main peak at m/z (pos.) = 663.2 ([Mn^{II}L(fla)]K^+) for **1**, 626.2 ([Fe^{II}L(fla)]H^+) for **2**, 667.2 ([Co^{II}L(fla)]K^+) for **3**, 650.3 ([Ni^{II}L(fla)]Na^+) for **4**, 633.3 ([Cu^{II}L(fla)]H^+) for **5**, and 634.1 ([Zn^{II}L(fla)]H^+) for **6**, respectively (Table 3) but did not give any carboxylate or flavonolate bridged dimer peak. Since the iron(II) complex [Fe^{II}L(fla)] (**2**) was very sensitive to air in solution, we obtained the overlapped peaks of [Fe^{III}L(fla)]$^+$ (m/z (pos.) = 625.2) and [Fe^{II}L(fla)]H^+ (m/z (pos.) = 626.2) when the sample was prepared in a glove box and measured under air (Supporting Information Figure S3a), but we did not observe any oxo or flavonolate bridged dimer structure. Such the auto-oxidation products were not detected in the case of other complexes, indicating that the complexes are relatively stable under air in solution and remaining their oxidation state except the Fe(II)-complex, being consistent with EPR and CV results described below. The m/z values and the isotope distribution patterns of all the peaks are in good agreement with the calculated values. These results indicate that the complexes remain their mononuclear structures in solution, which is consistent with the solution FT-IR, solution EPR, and solution magnetic moment results.

Solution EPR Spectroscopy. The X-band EPR spectra of the Mn, Fe, Co, and Cu-complexes in DMF were examined under N_2 at 100 K (Supporting Information Figure S4). Complex [Fe^{II}L(fla)] (**2**) was EPR silent under N_2 (Supporting Information Figure S4a-A), indicating that the Fe(II)-complex is in the low-spin oxidation state, which is similar to the spin state of Fe^{II} in the native enzyme[6a] and other Fe^{II}−quercetin complexes.[27]

The EPR spectrum of [Cu^{II}L(fla)] (**5**) displayed a typical axial symmetry signal with the EPR parameters of $g_{//}$ = 2.25, $g_\perp$ = 2.06, $A_{//}$ = 159 G (Supporting Information Figure S4c-A, the parameters were obtained by the simulation using a WIN EPR software), which are similar to those of the enzyme-flavonol adduct ($g_{//}$ = 2.31 and $A_{//}$ = 142 G, square pyramidal geometry with a monodentate coordinated substrate) from *A. japonicus*,[28] suggesting that [Cu^{II}L(fla)] also has a similar mononuclear square pyramidal geometry with a monodentate coordinated substrate flavonolate. The observed g value ($g_{//} > g_\perp > g_e$) are typical for a mononuclear copper(II) ($3d^9$) ion in axial symmetry geometry with the unpaired electron lying in the $d_{x^2-y^2}$ orbital at the ground state.[29]

The EPR spectrum of [Mn^{II}L(fla)] (**1**) displayed a strong 6-fold hyperfine splitting centered at g = 2.01 with a hyperfine coupling constant of 95 G (Supporting Information Figure S4d-A), corresponding to the $+^1/_2 \rightarrow -^1/_2$ transition of the $^5/_2$ spin of ^{55}Mn. This clearly indicates that complex **1** is a typical octahedrally coordinated monomuclear Mn^{II} complex with nitrogen and oxygen donors.[30] The spectral data are also very similar to those of the native Mn^{II}-containing enzyme (g = 2.0, A = 93 G; g = 9.0, A = 92 G) and its ES adduct from *B. subtilis*,[6a] suggesting that [Mn^{II}L(fla)] (**1**) also has a mononuclear distorted octahedral geometry.

The EPR spectrum of [Co^{II}L(fla)] (**3**) showed a very week signal (Supporting Information Figure S4e-A) at $g \sim$ 5.60 and 2.25, which is similar to that of the native high-spin Co^{II}-containing enzyme and its ES adduct from *Streptomyces* sp. FLA (g = 6.0, A = 95 G; g = 3.8 and 2.3)[6b] and *B. subtilis* (g = 6.5).[6a] However, the signal is too week at the liquid nitrogen temperature to be analyzed in detail.

Solution Magnetic Moment. The solution magnetic susceptibility of the paramagnetic complexes were examined by NMR using Frei−Bernstein's method,[31] with TMS as a reference and $CDCl_3$ as a solvent. The solution magnetic moments of the paramagnetic complexes were calculated and listed in Table 3. The magnetic moments of the paramagnetic Mn^{II}-, Co^{II}-, Ni^{II}-, Cu^{II}-complexes are 5.94, 4.13, 3.12, and 1.99 μ_B, respectively, which are consistent with or a little larger (due to the contribution of the orbital moment) than the corresponding calculated values using the spin-only equation of the high-spin Mn^{II} (5.92 μ_B), Co^{II} (3.87 μ_B), Ni^{II} (2.83 μ_B), and Cu^{II} (1.73 μ_B) centers, respectively, but in the range of the experimental data Mn^{II} (4.3−5.2 μ_B), Co^{II} (4.3−5.2 μ_B), Ni^{II} (2.8−3.5 μ_B), Cu^{II} (1.7−2.2 μ_B), respectively. Since the diamagnetic (low-spin) [Fe^{II}L(fla)] was very air-sensitive in solution, we observed some paramagnetically shifted reference resonance due to the auto-oxidation of Fe(II) to Fe(III) during measurement. In order to get insight into the nature of the Fe(III)-complex that initially formed upon reaction with O_2, we reexamined [Fe^{II}L(fla)] solution after exposure to O_2 for 10 min. The magnetic moment is 5.79 μ_B, which is similar to the Fe(III) analogue [Fe^{III}L(fla)](OAc) (**2A**) (5.76 μ_B, Supporting Information Table S4) and is in line with the calculated value using the spin-only equation of the high-spin Fe^{III} center (5.92 μ_B), indicating that [Fe^{II}L(fla)] is oxidized to high-spin [Fe^{III}L(fla)]$^+$ by O_2 and keeps a mononuclear structure in solution even after oxidation. These results also indicate that our model complexes keep their oxidation state (except Fe) and a mononuclear structure in solution.

^{1}H NMR Spectroscopy. ^{1}H NMR spectra of the Fe(II)-, Co(II)-, Ni(II)-, and Zn(II)-complexes were examined in $CDCl_3$ for **2** and **6**, and in d^7-DMF for **3** and **4** at ambient temperature (Supporting Information Figure S5). Both spectra of the paramagnetic Co(II)- and Ni(II)-complexes contain several paramagnetically shifted weak and broad resonances over a range of −7−17 ppm, which are similar to those of the corresponding [M^{II}(6-Ph_2TPA)(fla)]ClO_4 (M = Co and Ni),[13a] respectively. Since [Fe^{II}L(fla)] was very air sensitive in solution, we observed several paramagnetically shifted weak and

dx.doi.org/10.1021/ic400972k | *Inorg. Chem.* 2013, 52, 10936−10948

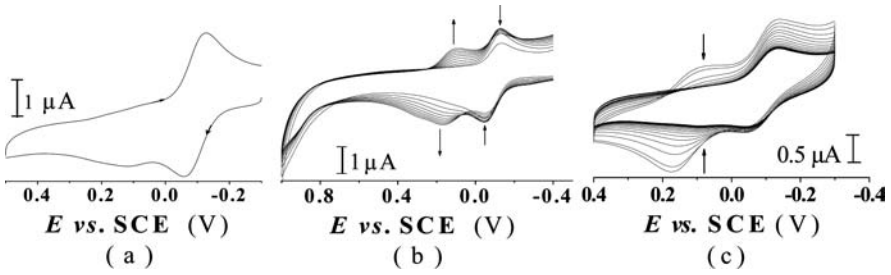

Figure 3. Cyclic voltammograms of $[Fe^{II}L(fla)]$ in DMF at room temperature: (a) under N_2, when (b) appearance and (c) disappearance of the second couple under slightly aerobic condition.

Scheme 2. Reaction of the Model Complexes with O_2 and Their Reaction Products

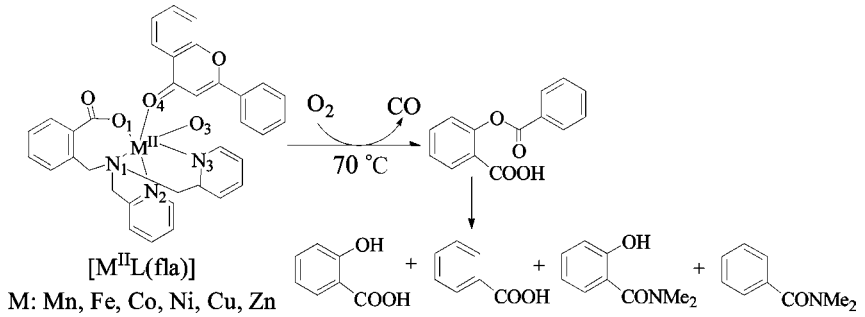

broad resonances over a range of −7−17 ppm due to the auto-oxidation of Fe(II) to Fe(III) during the measurement, which is also similar to that of $[Fe^{II}(6\text{-}Ph_2TPA)(fla)]ClO_4$.[13a]

Cyclic Voltammetry. The redox properties of $[M^{II}L(fla)]$ were examined by cyclic voltammetry at room temperature under N_2. The results are summarized in Table 3. All potentials are reported versus SCE. There is a quasi-reversible redox couple in the Fe(II)-complex $[Fe^{II}L(fla)]$ (**2**) at $E_{1/2}$ = −0.094 V (ΔE_p = 69 mV, i_{pc}/i_{pa} = 1.00) (Figure 3a), which can be assigned to the one-electron oxidation from Fe^{II} to Fe^{III}. The $E_{1/2}$ value of the $[Fe^{III/II}L(fla)]^{+/0}$ couple is more negative than that of $[(6\text{-}Ph_2TPA)Fe^{III/II}(fla)]^{2+/+}$ (+0.35 V)[13a] due to the existing negative charge (carboxylate) in the present ligand system L^-. The Co(II)-complex $[Co^{II}L(fla)]$ (**3**) also has a quasi-reversible redox couple at $E_{1/2}$ = −0.062 V (ΔE_p = 201 mV, i_{pc}/i_{pa} = 0.94) under O_2 (Supporting Information Figure S6a), which can be assigned to the one-electron oxidation from Co^{II} to Co^{III}. In $[Cu^{II}L(fla)]$ (**5**), a quasi-reversible redox couple appeared at $E_{1/2}$ = −0.427 V (ΔE_p = 120 mV, i_{pc}/i_{pa} = 2.32), which can be assigned to one-electron reduction of Cu^{II} to Cu^{I} (Figure S6c). The $E_{1/2}$ value of $[Cu^{II/I}L(fla)]^{0/-}$ couple is similar to that of $[Cu^{II}(6\text{-}Ph_2TPA)(fla)]OTf$ (−0.500 V, ΔE_p = 377 mV).[13a] The i_{pc}/i_{pa} value of $[Cu^{II/I}L(fla)]^{0/-}$ is large, which is similar to that of $[Cu^{II}(6\text{-}Ph_2TPA)(fla)]OTf$ (i_{pc}/i_{pa} ∼ 3).[13a] Such the metal redox couple were not observed with the Mn^{II}-, Ni^{II}-, and Zn^{II}-complexes within the range of −1.5−+1.5 V.

Interestingly, when a DMF solution of $[Fe^{II}L(fla)]$ (**2**) was contacted slowly with O_2, a quasi-reversible redox couple at $E_{1/2}$ = +0.130 V (ΔE_p = 78 mV, i_{pc}/i_{pa} = 1.05) appeared (Figure 3b) then disappeared (Figure 3c) slowly, which was not observed under anaerobic conditions. In fact, a new absorption band arose at 670 nm (Supporting Information Figure S7−blue line) (same with reported free $fla^{\bullet}$ at 676 nm[26a]) in Fe-complexes during the CV measurement under O_2, which could be assigned to the flavonoxy radical $fla^{\bullet}$ generated in a one-electron oxidation of fla^-. This redox couple observed in the slow oxygenation reaction could be tentatively assigned to one-electron oxidation from fla^- to $fla^{\bullet}$ on the O_2-generated $[Fe^{III}L(fla)]^+$. The redox couple of fla^- to $fla^{\bullet}$ were also observed in the Co^{II}-complexes at $E_{1/2}$ = +0.306 V (ΔE_p = 180 mV, i_{pc}/i_{pa} = 0.94) (Supporting Information Figure S6b). In other complexes $[M^{II}L(fla)]$ (M = Mn, Ni, Cu, and Zn), we only observed an irreversible oxidation wave but did not observe any reduction wave of the $fla^{\bullet}$ to fla^- even under O_2. The oxidation wave of the fla^- to $fla^{\bullet}$ appeared at +0.469 V for $[Mn^{II}L(fla)]$ (**1**), +0.169 V for $[Fe^{II}L(fla)]$ (**2**), +0.396 V for $[Co^{II}L(fla)]$ (**3**), +0.401 V for $[Ni^{II}L(fla)]$ (**4**), +0.243 V for $[Cu^{II}L(fla)]$ (**5**), and +0.438 V for $[Zn^{II}L(fla)]$ (**6**), respectively. The oxidation potential E_{pa} of the coordinated flavonolate of the complexes are much negative than those of reported $[M^{II}(6\text{-}Ph_2TPA)(fla)]OTf$ (M = Mn, Fe, Ni, Cu, and Zn) (+0.765 ∼ +1.06 V in CH_2Cl_2)[13a] (Mn: +0.765 V, Ni: +0.906 V, Cu: +1.06 V, and Zn: +0.934 V, respectively), $[Fe^{II}(fla)(H_2O)_4]Cl$ (+0.84 V), and $[Cu^{II}(fla)(H_2O)_2]Cl$ (+0.87 V) (in MeOH), respectively,[32] due to the existing negative charge of carboxylate in the supporting ligand L^-. Namely, the bound flavonolate are more easily oxidized in our model system.

The E_{pa} of the coordinated flavonolate of the complexes are in the range of +0.169−+0.469 V (over a range of 300 mV) and in the order of Fe (**2**) < Cu (**5**) < Co (**3**) < Ni (**4**) < Zn (**6**) < Mn (**1**), which is just reverse with the order of the Lewis acidity order of the metal ion (Zn^{II} < Cu^{II} > Ni^{II} > Co^{II} > Fe^{II} > Mn^{II}) provided by the Irving−Williams series[33] except Fe^{II} and Co^{II}. The Lewis acidity of the Co^{II} and Fe^{II} are weaker than Ni^{II} but the Fe^{II} (low-spin) and Co^{II} (high-spin) become to the stronger Fe^{III} (high-spin) and Co^{III} (low-spin), respectively, during reaction. $[Fe^{II}L(fla)]$ and $[Mn^{II}L(fla)]$ have the lowest and highest potential, respectively, indicating that the flavonolate is a better and worse reductant toward O_2 in $[Fe^{II}L(fla)]$ and $[Mn^{II}L(fla)]$, respectively, than in other M^{II}-complexes $[M^{II}L\text{-}(fla)]$. These results indicate that the E_{pa} of the bound substrate flavonolate are remarkably influenced by the Lewis acidity of

dx.doi.org/10.1021/ic400972k | Inorg. Chem. 2013, 52, 10936−10948

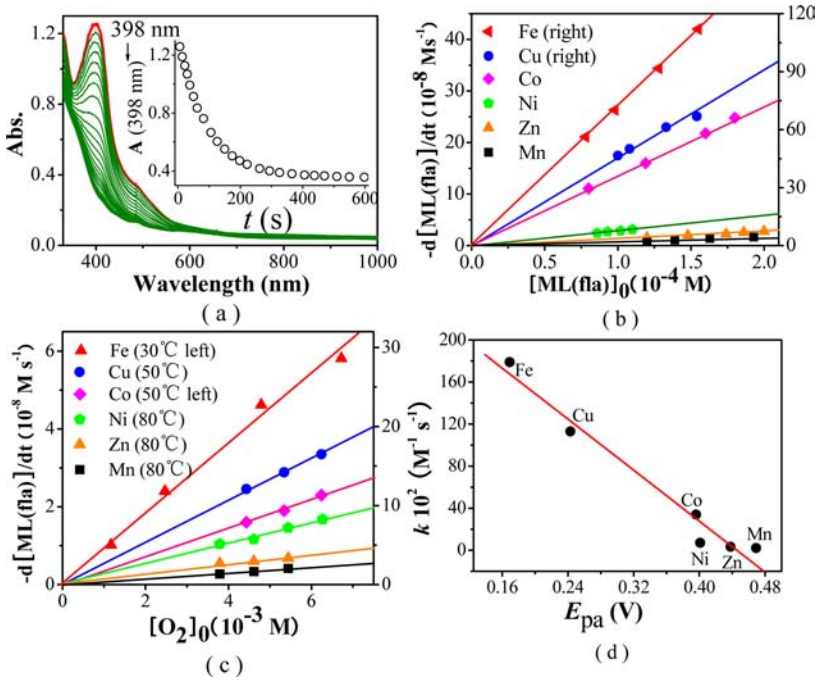

Figure 4. Dioxygenation of the $[M^{II}L(fla)]$ complexes at 70 °C under O_2. (a) Spectral change observed upon introduction of O_2 gas into a DMF solution of $[Fe^{II}L(fla)]$ (1.0×10^{-4} M). (inset) Time course of the absorption changes of $[Fe^{II}L(fla)]$ at 398 nm. (b) Plot of $-d[M^{II}L(fla)]/dt$ vs $[M^{II}L(fla)]_0$ ($\times 10^{-4}$ M at 70 °C). (c) Plot of $-d[M^{II}L(fla)]/dt$ vs $[O_2]_0$ ($\times 10^{-3}$ M). (d) Plot of k vs E_{pa} of the flavonolate.

the M^{II} ion, and the stronger Lewis acidity of the metal ion, the lower oxidation potential E_{pa} of the coordinated flavonolate of the complexes.

Degradation of Complexes (Enzyme-like Dioxygenation Reactivity). The ES model complexes $[M^{II}L(fla)]$ reacted with O_2 in DMF at 70 °C to give *o*-benzoylsalicylic acid (HObs) (*m*/*z* (pos.): 243 $(M + H)^+$) (1.9–21%) (Supporting Information Figure S8b) and CO (over 68% for **2**) (Supporting Information Figure S9) as the primary products (Supporting Information Table S2). The HObs was then hydrolyzed with a small amount of water in the solvent and amidated by the solvent DMF to give salicylic acid (*m*/*z* (neg.): 137 $(M - H)^-$) (79–97%) (Supporting Information Figure S8c and Figure S10a), benzoic acid (*m*/*z* (neg.): 121 $(M - H)^-$) (34–95%) (Supporting Information Figure S8d and Figure S10b), 2-hydroxy-*N*,*N*-dimethylbenzamide (*m*/*z* (pos.): 183 $(M + NH_4)^+$) (0–7.0%), and *N*,*N*-dimethylbenzamide (*m*/*z* (pos.): 150 $(M + H)^+$) (0.1–56%) as the final products (Scheme 2) (characterized by HPLC-MS and HPLC results) (Table S2 and Figures S8 and S10). The conversion of the model complexes are over 95%. Two main reaction products salicylic acid and benzoic acid were also identified by ^1H NMR after esterification and separation (Figure S10). The spectra of the products were identical to those of the authentic samples (AIST: Integrated Spectral Database System of Organic Compounds. (Data were obtained from the National Institute of Advanced Industrial Science and Technology, Japan)). Since the yields of other reaction products were low, we could not isolate and characterize them further. The dioxygenation reaction products of our model complexes are very similar to the reaction products of the native enzyme, indicating that our model complexes $[M^{II}L(fla)]$ have enzyme-like dioxygenation reactivity.

The dioxygenation of the complexes were followed by monitoring the disappearance of the band due to the $\pi \rightarrow \pi^*$ transition of the coordinated flavonolate at the corresponding λ_{max} (Figure 4a for $[Fe^{II}L(fla)]$, Supporting Information Figure S2 and Table 3). The kinetic data and activation parameters of the complexes are listed in Table 4 and Supporting Information Table S3. The plots of the initial reaction rate versus the initial concentration of both $[M^{II}L(fla)]$ (Figure 4b) and dioxygen (Figure 4c) are linear, respectively. So the rate law can be described as $-d[M^{II}L(fla)]/dt = k[M^{II}L(fla)][O_2]$. The second-order reaction rate constants k were thus determined as 2.05–179 $\times 10^{-2}$ M^{-1} s^{-1} at 70 °C ($\Delta H^{\ddagger}$ = 55–84 kJ mol^{-1}, $\Delta S^{\ddagger}$ = −40 to −84 J mol^{-1} K^{-1}) (Table 4 and Supporting Information Table S3 and Figure S11). Reactivity of the reported 2,3-QD model complexes were much lower and required higher temperature (80–145 °C) (Table 5)[8–14,34] as compared with that of our complexes. The higher reactivity of the present model system could be attributed to the carboxylate group attached to the supporting ligand, which may enhance the reactivity via lowering the redox potential of the coordinated

Table 4. Kinetic Data (at 70 °C) and Activation Parameters of the Complexes

	10^2k (M^{-1} s^{-1})	$\Delta H^{\ddagger}$ (kJ mol^{-1})	$\Delta S^{\ddagger}$ (J mol^{-1} K^{-1})	E_a (kJ mol^{-1})
[MnL(fla)] (**1**)	2.05 ± 0.13	69.94	−75.82	72.88
[FeL(fla)] (**2**)	179 ± 0.08	65.92	−51.81	68.60
[CoL(fla)] (**3**)	34.0 ± 0.04	84.48	−8.290	87.27
[NiL(fla)] (**4**)	7.11 ± 0.16	63.60	−82.19	66.51
[CuL(fla)] (**5**)	113 ± 0.03	55.25	−83.67	58.03
[ZnL(fla)] (**6**)	3.37 ± 0.10	80.72	−39.90	83.65

dx.doi.org/10.1021/ic400972k | *Inorg. Chem.* 2013, 52, 10936–10948

Table 5. Summary of the Kinetic Data for the Metal–Flavonolate Model Complexes

complexes	T (°C)	10^2k (M^{-1} s^{-1})	ref
[MnL(fla)] (**1**)	70	2.05	this work
[$Mn^{II}L^1$(fla)]	80	0.82	13c
[$Mn(fla)_2Py_2$]	100	50.0	11
[Fe^{II}L(fla)] (**2**)	70	179	this work
[$Fe^{II}L^1$(fla)]	80	58.6	13c
[$Fe^{III}(fla)_3$]	100	80.0	11
[Fe^{III}(fla)(salen)]	100	2.07	9b
[Co^{II}L(fla)] (**3**)	70	34.0	this work
[$Co^{II}L^1$(fla)]	80	2.09	13c
[Co^{III}(fla)(salen)]	25	v = 5.50 × 10^{-6} M s^{-1}	12
[NiL(fla)] (**4**)	70	7.11	this work
[$Ni^{II}L^1$(fla)]	80	0.43	13c
[CuL(fla)] (**5**)	70	113	this work
[$Cu^{II}L^1$(fla)]	80	1.34	13c
[Cu^{II}(Bz-tac)(fla)]ClO_4	120	0.331	34a
[Cu^{II}(fla)(ipr-tac)]ClO_4	120	0.151	34a
[Cu^{II}(fla)(idpaH)]ClO_4	100	0.613	34b
[$Cu^{II}(fla)_2$]	100	1.57	34c
[$Cu^{II}(fla)_2$(tmeda)]	80	2.40	34d
[$Cu^{II}(fla)_2$(bpy)]	80	2.02	34d
[$Cu^{II}(fla)_2$(phen)]	80	9.50	34d
[Cu^{II}(fla)$(phen)_2$]ClO_4	120	18.3	34d
[ZnL(fla)] (**6**)	70	3.37	this work
[Zn^{II}(fla)(idpa)] ClO_4	100	0.311	14

flavonolate by electron-donation. Notably, the reactivity of [Fe^{II}L(fla)] and [Cu^{II}L(fla)] were quite high (k = 1.79 and 1.13 M^{-1} s^{-1} at 70 °C, respectively) over the other divalent metal complexes. Maybe it is because the Fe(II)-complex is easily auto-oxidized to form more Lewis acidic and reactive Fe(III)-complex during reaction with O_2, and in [Cu^{II}L(fla)] the flavonolate ligand is coordinated via more reactive monodentate coordination mode (based on EPR results) and the Lewis acidity of the Cu(II) is stronger than others.

Although the structures of the ES-model complexes [M^{II}L-(fla)] are similar, the reactivity of the [M^{II}L(fla)] complexes toward dioxygen were significantly different as in the order of Fe (**2**) > Cu (**5**) > Co (**3**) > Ni (**4**) > Zn (**6**) > Mn (**1**) (Figure 4), which is just reverse with the order of oxidation potential E_{pa} of the coordinated flavonolate of the complexes, and the plot of k vs E_{pa} is linear (R = 0.98) (Figure 4d). This order is also approximately consistent with the Lewis acidity order of the metal ion (Zn^{II} < Cu^{II} > Ni^{II} > Co^{II} > Fe^{II} > Mn^{II}) and the Irving–Williams series except Fe^{II} and Co^{II}. This tendency is similar to those seen in the enzyme system[6a] and other enzymatic and nonenzymatic systems such as RNA catalysis[35a] and metal ion catalysis for the decomposition of tetramethyl-1,2-dioxetane.[35b] The observed differences in the reactivity among them may be attributed to the Lewis acidity of the metal ion and its coordination environment. Maybe the metal(II) ion could be to adjust the orientation of the bound substrate flavonolate and the coordination environment of the M^{II} ion, to control the redox potential of the flavonolate, and to stabilize the flavonoxyl radical electrostaticly, which is similar to the enzymatic system.[6b] These results indicate that the stronger Lewis acidity of the metal ion, the lower oxidation potential E_{pa} of the coordinated flavonolate and the higher dioxygenation reactivity. Our study is the first example of the metal ion effects on the enzyme-like dioxygenation reactivity of a series of structural and functional ES model system, providing important insights into the metal ion effects on the enzymatic reactivity of metal-substituted 2,3-QD.

Catalytic Mechanism. Importantly, when the complexes [M^{II}L(fla)] were treated with O_2 in the presence of excess nitro blue tetrazolium (NBT^{2+}), a new absorption band arose at 530 nm (Figure 5–blue line), indicating that [M^{II}L(fla)] reacted with O_2 to produce free $O_2^{\bullet-}$ (superoxide radical) and NBT^{2+} was reduced to monoformazan (MF^+) by the generated $O_2^{\bullet-}$.[36]

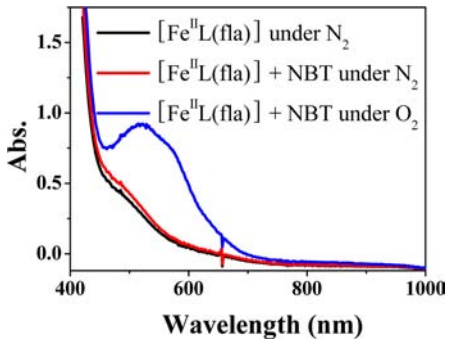

Figure 5. Spectral change of [Fe^{II}L(fla)] (0.5 mM in DMF) under N_2 (black) and in the presence of NBT under N_2 (red) and O_2 (blue) at rt.

The ESI-MS and ESR results of the complexes obtained after exposure to air or O_2 and after the reaction with O_2 were summarized in Table 6. When the solution of [Fe^{II}L(fla)] (**2**) and [Co^{II}L(fla)] (**3**) were exposed to air and O_2, we initially observed a peak cluster due to [Fe^{III}L(fla)]$^+$ at m/z (pos.) = 625.2 (Supporting Information Figure S3b) and [Co^{III}L(fla)]$^+$ at m/z (pos.) = 628.2 (Supporting Information Figure S13b), respectively, and a typical mononuclear Fe^{III} signal with g = 8.02, 4.24, and 2.20 (Supporting Information Figure S4a-B and S4b), indicating that the Fe(II) and Co(II) were oxidized by O_2 to Fe^{III} and Co^{III} at the first stage of the reaction. After the [Fe^{II}L(fla)] solution was exposed to O_2 for 5 min, about 87% Fe^{II} was converted to Fe^{III} (Figure S4b) based on the peak area relative to the external standard [$Fe^{III}L^{OMe}(sal^{2-})$] ($L^{OMe}$: p-OMe substituted at the benzoic side arm of the ligand L, sal: salicylate, unpublished results), which also has a similar mononuclear distorted octahedral structure (characterized by single crystal X-ray diffraction, EA, ESI-MS, et al.). After the reaction with O_2, we observed a peak cluster due to [$Fe^{III}L(sal^{2-})$]H^+ (sal: salicylate, one of the oxidation products) at m/z (pos.) = 525.3 for [Fe^{II}L(fla)] (**2**) and [Co^{III}L(ben)]$^+$ (ben: benzonate, one of the oxidation products) at m/z (pos.) = 512.1 for [Co^{II}L(fla)] (**3**), respectively, and a typical mononuclear Fe(III) signal at g = 7.66, 4.27, and 2.06 (Supporting Information Figure S4a-C), and the weak Co^{II} EPR signal disappeared (Supporting Information Figure S4e-B).

In order to get insight into the nature of the Fe(III)- and Co(III)-complexes that initially formed upon reaction with O_2, the Fe(III) and Co(III) analogues [M^{III}L(fla)](OAc) (M = Fe (**2A**), Co (**3A**)) were synthesized independently and characterized (Supporting Information page S4: synthesis of the M^{III}-complexes [M^{III}L(fla)](OAc) (M = Fe (**2A**), Co (**3A**)); Supporting Information Table S4 and Figure S12 and S13). The λ_{max} of the $\pi \rightarrow \pi^*$ transition of the coordinated flavonolate of the complexes are 406 nm for **2A** (Supporting Information Figure S12a) and 425 nm for **3A** (Supporting

dx.doi.org/10.1021/ic400972k | Inorg. Chem. 2013, 52, 10936–10948

Table 6. ESI-MS and ESR Results of the Complexes when Exposed to Air or O_2 and After the Reaction with O_2

	ESI-MS (m/z (pos.))		EPR (g, A)	
	exposed to air/O_2	after reaction	exposed to O_2	after reaction
$[Mn^{II}L(fla)]$ (**1**)		536.3 ($[Mn^{II}L(dmb)]^+$)		g = 2.06, A = 90.5 G, g = 6.12, 16.4
$[Fe^{II}L(fla)]$ (**2**)	625.2 ($[Fe^{III}L(fla)]^+$)	525.3 ($[Fe^{III}L(sal^{2-})]H^+$)	g = 8.02, 4.24, 2.20	g = 7.66, 4.27, 2.06
$[Co^{II}L(fla)]$ (**3**)	628.2 ($[Co^{III}L(fla)]^+$)	512.1 ($[Co^{III}L(ben)]^+$)		no signal
$[Cu^{II}L(fla)]$ (**5**)		565.4 ($[Cu^{II}L(sal^-)]$ $H^+{\cdot}CH_3OH$)		$g_{//}$ = 2.26, $g_\perp$ = 2.07, $A_{//}$ = 195 G

Scheme 3. Proposed Dioxygenation Reaction Mechanism of the Model Complexes $[M^{II}L(fla)]$

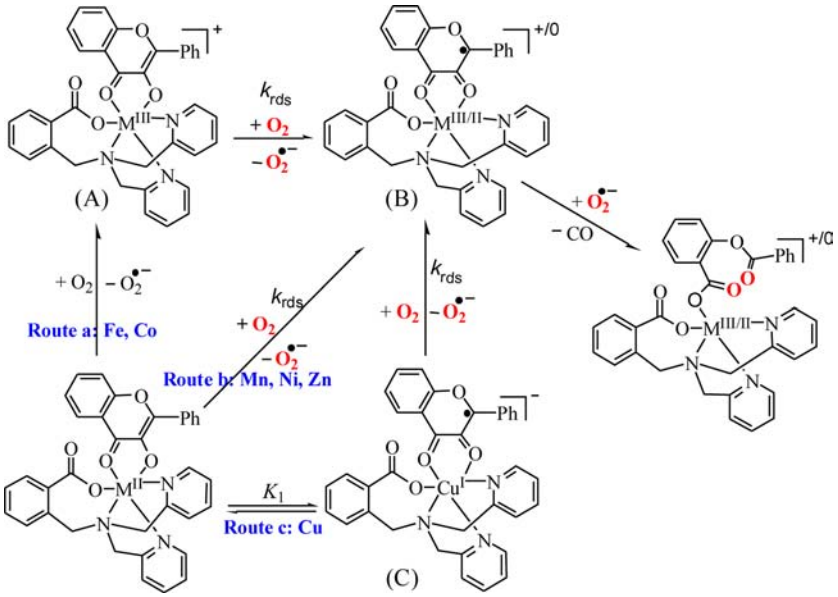

Information Figure S13a), respectively. Both **2A** and **3A** are 8 nm red-shifted than those of the corresponding M(II) analogues $[M^{II}L(fla)]$ (398 nm for **2** and 417 nm for **3**), respectively. The wavelength of $[Fe^{III}L(fla)](OAc)$ (**2A**) is similar to the initially formed $[Fe^{III}L(fla)]^+$. The magnetic moments of $[M^{III}L(fla)](OAc)$ are 5.76 μ_B for **2A** and 0.45 μ_B for **3A**, respectively, which are in good agreement with the calculated values using the spin-only equation of the high-spin Fe^{III} (5.92 μ_B) and low-spin Co^{III} (0.00 μ_B) center, respectively. These results are consistent with the solution ESR results. The magnetic moment of $[Fe^{III}L(fla)](OAc)$ is similar to that of the initially formed Fe(III)-complex (5.79 μ_B) upon reaction with O_2. These results indicate that $[Fe^{II}L(fla)]$ and $[Co^{II}L(fla)]$ are oxidized to high-spin $[Fe^{III}L(fla)]^+$ and low-spin $[Co^{III}L(fla)]^+$, respectively, at the first stage during the reaction with O_2, and keep a similar mononuclear structure in solution. The reactivity of $[M^{III}L(fla)](OAc)$ toward dioxygen were also examined. The plots of the initial reaction rate versus the initial concentration of both $[M^{III}L(fla)](OAc)$ and dioxygen are also linear, respectively (Figure S12 for **2A** and Figure S13 for **3A**). So the rate law also can be described as $-d[M^{III}L(fla)(OAc)]/dt = k[M^{III}L(fla)(OAc)][O_2]$. The second-order reaction rate constants k of $[M^{III}L(fla)](OAc)$ are 133 × 10^{-2} M^{-1} s^{-1} ($\Delta H^{\ddagger}$ = 109 kJ mol^{-1}, $\Delta S^{\ddagger}$ = −52 J mol^{-1} K^{-1}) for **2A** at 50 °C and 71.2 × 10^{-2} M^{-1} s^{-1} ($\Delta H^{\ddagger}$ = 111 kJ mol^{-1}, $\Delta S^{\ddagger}$ = −75 J mol^{-1} K^{-1}) for **3A** at 70 °C (Supporting Information Table S3 and Figures S12 and S13), which are about 2−3 times larger than those of the corresponding M(II) analogues $[M^{II}L(fla)]$ (39.8 × 10^{-2} M^{-1} s^{-1} for **2** and 34.0 × 10^{-2} M^{-1} s^{-1} for **3**, respectively) at the same temperature. The enhanced reactivity of $[M^{III}L(fla)](OAc)$ could be attributed to the enhanced Lewis acidity of the M(III) ion and their coordination environment.

After the reaction of $[Mn^{II}L(fla)]$ (**1**) and $[Cu^{II}L(fla)]$ (**5**) with O_2, we observed a peak cluster due to $[Mn^{II}L(dmb)]^+$ (dmb: *N*,*N*-dimethyl-benzamide, one of the amidated oxidation product) at m/z (pos.) = 536.3 and $[Cu^{II}L(sal^-)]H^+{\cdot}CH_3OH$ at m/z (pos.) = 565.4, respectively, and a typical sextet mononuclear Mn^{II} signal with the EPR parameters of g = 2.06 (A = 90.5 G), g = 6.12, and 16.4 (Supporting Information Figure S4d-B) and $g_{//}$ = 2.26, $g_\perp$ = 2.07, $A_{//}$ = 195 G (Figure S4c-B), respectively.

In the Mn^{II}-, Ni^{II}-, and Zn^{II}-complexes, we did not observe any metal ion redox couple during CV measurements even under O_2. When the complexes were exposed to O_2 or reacted with O_2, we did not observe any oxidation state change on ESI-MS and EPR. These results indicate that the Mn^{II}-, Ni^{II}-, and Zn^{II}-complexes are stable toward O_2 in solution and keep their oxidation state during reaction.

On the basis of the spectroscopic and kinetic results, we suggest the dioxygenation mechanism of $[M^{II}L(fla)]$ as follows (Scheme 3).

Fe^{II}- and Co^{II}-complexes $[M^{II}L(fla)]$ (M = Fe and Co) (Scheme 3−route a): $[M^{II}L(fla)]$ may react with one O_2 molecule to produce $[M^{III}L(fla)]^+$ (A) and $O_2^{\bullet-}$ quickly. Then $[M^{III}L(fla)]^+$ reacts with another O_2 molecule to generate flavonoxy radical $[M^{III}L(fla^{\bullet})]$ (B) and superoxide radical slowly by direct one electron transfer from the coordinated substrate fla^- to O_2, which are similar to the enzymatic system.[6a] Then B reacts with $O_2^{\bullet-}$ quickly and releases CO.

Mn^{II}-, Ni^{II}-, and Zn^{II}-complexes $[M^{II}L(fla)]$ (M = Mn, Ni, and Zn) (Scheme 3−route b): The reaction mechanism of

dx.doi.org/10.1021/ic400972k | Inorg. Chem. 2013, 52, 10936−10948

these complexes are similar to Fe^{II}- and Co^{II}-complexes except the first step, and there is direct one electron transfer from the activated flavonol (fla^-) to dioxygen to generate flavonoxy radical $[M^{II}L(fla^{\bullet})]$ (B) and superoxide radical slowly.

For the copper(II)-complex $[Cu^{II}L(fla)]$ (Scheme 3—route c), there is a fast equilibrium between $[Cu^{II}L(fla)]$ and $[Cu^{I}L(fla^{\bullet})]$ (C), which is more favorable than dioxygen activation. Then $[Cu^{I}L(fla^{\bullet})]$ react with one O_2 molecule to form $[Cu^{II}L(fla^{\bullet})]$ (B) and superoxide radical slowly by direct one electron transfer from Cu^{I} to O_2. Then B reacts with $O_2^{\bullet-}$ quickly and releases CO.

The reaction mechanism of $[Cu^{II}L(fla)]$ is similar to the Cu^{II}-containing 2,3-QD,[2−4] and the reaction mechanism of $[M^{II}L(fla)]$ (M = Fe, Mn, Co, and Ni) are similar to the Fe(II)-, Mn(II)-, Co(II)-, and Ni(II)-containing 2,3-QD, respectively.[5,6] It is very similar to the intradiol and extradiol catechol dioxygenase, respectively.[37]

CONCLUSIONS

In conclusion, we succeeded in developing a series of structural and functional ES models of the metal flavonolate complexes $[M^{II}L(fla)]$ (M = Mn (**1**), Fe (**2**), Co (**3**), Ni (**4**), Cu (**5**), and Zn (**6**)) for the active site of various metal(II)-containing 2,3-QD. The structures, spectroscopic features, redox properties, and the reactivity toward molecular oxygen have been investigated in detail. The reaction of the model complexes with O_2 exhibits first-order dependence with respect to both the complexes and dioxygen. The reaction of the complexes toward dioxygen show higher reactivity at lower temperature, which are greatly enhanced by the carboxylate group of the supporting ligand by electron donation. Thus, our complexes act as good functional ES models of various metal(II)-containing 2,3-QD. The reactivity of the $[M^{II}L(fla)]$ complexes show notable differences and it is in the order of Fe (**2**) > Cu (**5**) > Co (**3**) > Ni (**4**) > Zn (**6**) > Mn (**1**). The differences on the reactivity among them may be attributed to the redox potential of the coordinated flavonolate of the complexes, which are remarkably influenced by the Lewis acidity of the metal ion and its coordination environment. Our complexes $[Fe^{II}L(fla)]\cdot H_2O$ (**2**), $[Co^{II}L(fla)]\cdot CH_3OH$ (**3**), and $[Ni^{II}L(fla)]$ (**4**) are the first structurally characterized Fe^{II}-, Co^{II}-, and Ni^{II}-flavonolate ES model complexes of Fe^{II}-, Co^{II}-, and Ni^{II}-containing 2,3-QD, respectively. Our study is the first example of the metal ion effects on the enzyme-like dioxygenation reactivity and a series of good structural and functional models of various metal(II)-containing 2,3-QD, providing important insights into the metal ion effects on the enzymatic reactivity of metal-substituted 2,3-QD.

ASSOCIATED CONTENT

Supporting Information

The FT-IR, UV—vis, ESI-MS, EPR, ^1H NMR, CV, LC-MS spectra, Eyring plot, reaction products analysis data, kinetic data, and crystallographic information (CIF) CCDC 840052 for **2**, CCDC 840051 for **3**, and CCDC 948142 for **4**, respectively. This material is available free of charge via the Internet at http://pubs.acs.org.

AUTHOR INFORMATION

Corresponding Author

*E-mail: yingjis@dlut.edu.cn.

Notes

The authors declare no competing financial interest.

ACKNOWLEDGMENTS

We thanks a lot Prof. Sugimoto Hideki (Osaka Univ., Japan) for his kind help in crystal structure analysis. We are gratefully acknowledged the financial support of the National Natural Science Foundation of China (No. 20641002, 20771020, 20811140328) and the postdoctoral fellowship of JSPS (Japan Society for the Promotion of Science).

REFERENCES

(1) Wollenweber, E. *Flavonoids: Advances in Research*; Harborne, J. B., Mabry, T. J., Eds.; Chapman&Hall: London, UK, 1982.
(2) Fusetti, F.; Schröter, K. H.; Steiner, R. A.; van Noort, P. I.; Pijning, T.; Rozeboom, H. J.; Kalk, K. H.; Egmond, M. R.; Dijkstra, B. W. *Structure* **2002**, *10*, 259−268.
(3) Steiner, R. A.; Kalk, K. H.; Dijkstra, B. W. *Proc. Natl. Acad. Sci.* **2002**, *99*, 16625−16630.
(4) (a) Steiner, R. A.; Kooter, I. M.; Dijkstra, B. W. *Biochemistry* **2002**, *41*, 7955−7962. (b) Antonczak, S.; Fiorucci, S.; Golebiowski, J.; Cabrol-Bass, D. *Phys. Chem. Chem. Phys.* **2009**, *11*, 1491−1501.
(5) (a) Gopal, B.; Madan, L. L.; Betz, S. F.; Kossiakoff, A. A. *Biochem.* **2005**, *44*, 193−201. (b) Laura, B.; Shirley, A. F.; Victoria, J. J.; Stephen, B. *FEBS Lett.* **2004**, *557*, 45−48. (c) Barney, B. M.; Schaab, M. R.; LoBrutto, R.; Francisco, W. A. *Protein Expr. Purif.* **2004**, *35*, 131−141.
(6) (a) Schaab, M. R.; Barney, B. M.; Francisco, W. A. *Biochemistry* **2006**, *45*, 1009−1016. (b) Merkens, H.; Kappl, R.; Jakob, R. P.; Schmid, F. X.; Fetzner, S. *Biochemistry* **2008**, *47*, 12185−12196.
(7) (a) Dai, Y.; Pochapsky, T. C.; Abeles, R. H. *Biochemistry* **2001**, *40*, 6379−6387. (b) Fielding, A. J.; Kovaleva, E. G.; Farquhar, E. R.; Lipscomb, J. D.; Que, L. J., Jr. *Biol. Inorg. Chem.* **2011**, *16*, 341−355.
(8) (a) Kaizer, J.; Balogh-Hergovich, E.; Czaun, M.; Casy, T.; Speier, G. *Coord. Chem. Rev.* **2006**, *222*, 2222−2233. (b) Pap, J. S.; Kaizer, J.; Speier, G. *Coord. Chem. Rev.* **2010**, *254*, 781−793. (c) Kaizer, J.; Pap, J. S; Speier, G. *Copper Dioxygenases. in Copper—Oxygen Chemistry*; Karlin, K. D., Shinobu, I., Eds.; John Wiley & Sons, Inc.: Hoboken, NJ, 2011; pp 23−52.
(9) (a) Balogh-Hergovich, É.; Kaizer, J.; Speier, G. *J. Mol. Catal. A* **2003**, *206*, 83−87. (b) Baráth, G.; Kaizer, J.; Speier, G.; Párkányi, L.; Kuzmann, E.; Vértes, A. *Chem. Commun.* **2009**, 3630−3632.
(10) (a) Aramice, Y. S.; Malkhasian, F. M. E.; Nikolovski, B.; Menon, A.; Kucera, B. E.; Chavez, F. A. *Inorg. Chem.* **2007**, *46*, 2950−2952. (b) Kaizer, J.; Góger, S.; Speier, G.; Réglier, M.; Giorgi, M. *Inorg. Chem. Commun.* **2006**, *9*, 251−254.
(11) (a) Kaizer, J.; Barath, G.; Pap, J. S.; Speier, G. *Chem. Commun.* **2007**, 5235−5237. (b) Kaizer, J.; Pap, J. S.; Speier, G. *On Biomimetics*; Pramatarova, L. D., Eds.; Intech Open Access Publisher: New York, 2011, pp 29−42.
(12) Hiller, W.; Nishinaga, A.; Rieker, A. *Z. Naturforsch., B: Chem. Sci.* **1992**, *47*, 1185−1188.
(13) (a) Grubel, K.; Rudzka, K.; Arif, A. M.; Klotz, K. L.; Halfen, J. A.; Berreau, L. M. *Inorg. Chem.* **2010**, *49*, 82−96. (b) Grubel, K.; Laughlin, B. J.; Maltais, T. R.; Smith, R. C.; Arif, A. M.; Berreau, L. M. *Chem. Commun.* **2011**, *47*, 10431−10433. (c) Matuz, A.; Giorgi, M.; Speier, G.; Kaizer, J. *Polyhedron* **2013**, *63*, 41−49.
(14) Barhacs, L.; Kaizer, J.; Speier, G. *J. Mol. Catal. A* **2001**, *172*, 117−125.
(15) Armarego, W. L. F.; Perrin, D. D. *Purification of Laboratory Chemicals*, 4th ed.; Butterworth-Heinemann: Oxford, UK, 1996.
(16) Kruis, A. In *Landolt-Börnstein*; Springer-Verlag: Berlin, 1976; Board 4, Teil 4, pp 269.
(17) Ram, G.; Sharaf, A. R. *J. Ind. Chem. Soc.* **1968**, *45*, 13−16.
(18) Hemmert, C.; Verelst, M.; Tuchagues, J.-P. *Chem. Commun.* **1996**, 617−618.

(19) Amrani, F. B. A. E.; Perelló, L.; Real, J. A.; González-Alvarez, M.; Alzuet, G.; Borrás, J.; García-Granda, S.; Montejo-Bernardo, J. *J. Inorg. Biochem.* **2006**, *100*, 1208−1218.
(20) Brydon, P. *Ph. Mag. Lett.* **1999**, *79*, 383−387.
(21) Etter, M. C.; Urbanczyk-Lipkowska, Z.; Baer, S.; Barbara, P. F. *J. Mol. Struct.* **1986**, *144*, 155−167.
(22) Farina, Y.; Yamin, B. M.; Fun, H.-K.; Yip, B.-C.; Teoh, S.-G. *Acta Crystallogr.* **1995**, *C51*, 1537−1540.
(23) Christou, G.; Perlepes, S. P.; Libby, E.; Folting, K.; Huffman, J. C.; Webb, R. J.; Hendrickson, D. N. *Inorg. Chem.* **1990**, *29*, 3657−3666.
(24) Chadjistamatis, I.; Terzis, A.; Raptopoulou, C. P.; Perlepes, S. P. *Inorg. Chem. Commun.* **2003**, *6*, 1365−1371.
(25) Jurd, L.; Geissman, T. A. *J. Org. Chem.* **1956**, *21*, 1395−1401.
(26) (a) Barhács, L.; Kaizer, J.; Speier, G. *J. Org. Chem.* **2000**, *65*, 3449−3452. (b) Pap, J. S.; Matuz, A.; Baráth, G.; Kripli, B.; Giorgi, M.; Speier, G.; Kaizer, J. *J. Inorg. Biochem.* **2012**, *108*, 15−21.
(27) Guo, M.; Perez, C.; Wei, Y.; Rapoza, E.; Su, G.; Bou-Abdallah, F.; Chasteen, N. D. *Dalton Trans.* **2007**, 4951−4961.
(28) (a) Kooter, I. M.; Steiner, R. A.; Dijkstra, B. W.; van Noort, P. I.; Egmond, M. R.; Huber, M. *Eur. J. Biochem.* **2002**, *269*, 2971−2979. (b) Fittipaldi, M.; Steiner, R. A.; Matsushita, M.; Dijkstra, B. W.; Groenen, E. J. J.; Huber, M. *Biophys. J.* **2003**, *85*, 4047−4054.
(29) (a) Hathaway, B. J.; Tomlinson, A. A. G. *Coord. Chem. Rev.* **1970**, *5*, 1−43. (b) Hathaway, B. J.; Billing, D. E. *Coord. Chem. Rev.* **1970**, *5*, 143−207. (c) Yokoi, H. *Bull. Chem. Soc. Jpn.* **1974**, *47*, 3037−3040.
(30) Reed, G. H.; Markham, G. D. *Biological Magnetic Resonance*; Berliner, L. J., Reuben, J., Eds.; Plenum Press: New York, 1984; Vol. *6*, pp 73−142.
(31) (a) Freit, K.; Bernstein, H. J. *J. Chem. Phys.* **1962**, *37*, 1891−1892. (b) Kuchel, P. W.; Chapman, B. E.; Bubb, W. A.; Hansen, P. E.; Dur, C. J. *Concepts Magn. Reson.* **2003**, *A 18*, 56−71.
(32) De Souza, R. F. V.; Sussuchi, E. M.; De Giovani, W. F. *Synth. React. Inorg. Met.−Org. Chem.* **2003**, *33*, 1125−1144.
(33) Irving, H.; Williams, R. J. P. *J. Chem. Soc.* **1953**, 3192−3210.
(34) (a) Kaizer, J.; Pap, J.; Speier, G.; Párkányi, L. *Eur. J. Inorg. Chem.* **2004**, 2253−2259. (b) Barhács, L.; Kaizer, J.; Pap, J.; Speier, G. *Inorg. Chim. Acta* **2001**, *320*, 83−91. (c) Balogh-Hergovich, É.; Kaizer, J.; Speier, G.; Argay, G.; Párkányi, L. *J. Chem. Soc., Dalton Trans.* **1999**, 3847−3854. (d) Balogh-Hergovich, É.; Kaizer, J.; Pap, J.; Speier, G.; Huttner, G.; Zsolnai, L. *Eur. J. Inorg. Chem.* **2002**, 2287−2295.
(35) (a) Frederiksen, J. K.; Fong, R.; Piccirilli, J. A. Metal Ions in RNA Catalysis. In *RSC Biomolecular Sciences, Nucleic Acid-Metal Ion Interaction*; Hud, N. V., Eds.; Royal Society of Chemistry: London, 2009; Chapter 8, pp 260−306. (b) Dum, M. F.; Dietrich, H.; MacGibbon, A. K. H.; Koerber, S. C.; Zeppezauer, M. *Biochemistry* **1982**, *21*, 354−363.
(36) Blelski, B. H. J.; Shiue, G. G.; Bajuk, S. *J. Phys. Chem.* **1980**, *84*, 830−833.
(37) Bugg, T. D. H.; Lin, G. *Chem. Commun.* **2001**, 941−952.
(38) *Crystal Structure*, version 4.0; Rigaku Corp.: The Woodlands, TX, 2010.
(39) *Crystal Structure: Crystal Structure Analysis Package*, version 3.5.1; Rigaku Corp. and Molecular Structure Corp.: The Woodlands, TX, 2003.
(40) (a) *Program for the Solution of Crystal Structures*; University of Gottingen: Gottingen, Germany, 1997. (b) *Program for the Refinement of Crystal Structures*; University of Gottingen: Gottingen, Germany, 1997.
(41) Spek, A. L. *PLATON*, Multipurpose Crystallographic Tool, Utrecht University, Utrecht, The Netherlands, 2008.